




Science Paper

Balancing Redox Budgets: Mechanisms for Prolonging Anoxia During Major Carbon Burial Events

Sean M. Newby^{1,2}^a, Seth A. Young¹, Theodore R. Them II³, Benjamin C. Gill⁴, Jeremy D. Owens¹

¹ Earth, Ocean, and Atmospheric Science Department, National High Magnetic Field Laboratory, Florida State University, ² Department of Earth and Planetary Sciences, University of Hong Kong, ³ Department of Geology and Environmental Geosciences, College of Charleston, ⁴ Department of Geosciences, Virginia Polytechnic Institute and State University

Keywords: Toarcian Oceanic Anoxic Event, Oceanic Anoxic Event 2, Large Igneous Provinces, organic carbon burial, pyrite burial, oxidative weathering
<https://doi.org/10.2475/001c.143665>

American Journal of Science

Vol. 325, 2025

Widespread marine anoxic events occurred throughout the Phanerozoic, most notably the Mesozoic oceanic anoxic events (OAEs). They were likely the result of major climatic perturbations that resulted in the burial of significant quantities of organic matter-rich sediments. During OAEs, reduced carbon and sulfur are more efficiently sequestered, which, based on stoichiometric balances, should result in a net increase of oxygen counteracting marine deoxygenation. This relationship has been the fundamental basis of models for the long-term rise in oxygen across deep-time. However, the geologic record of OAEs indicate widespread marine anoxia persisted on million-year timescales while these processes occurred. Many OAEs occur contemporaneous with the emplacement of large igneous provinces (LIPs), which released volatile compounds that likely induced climatic perturbations that could, in turn, impact marine (de)oxygenation. These volcanic systems also released reducing compounds that may provide a mechanism for the temporal exacerbation of OAEs. Additionally, the climatic effects of LIPs are associated with enhanced chemical weathering intensities, which may have promoted increased oxidative weathering that also consumed oxygen. Here, forward box models provide first-order quantifications of the excess oxygen produced via organic carbon and pyrite sulfur burial along with the effects of introducing LIP-sourced reductants and oxidative weathering to the ocean-atmosphere system during OAEs. This study focuses on Oceanic Anoxic Event 2 (~94 Ma) and the Toarcian Oceanic Anoxic Event (~184 Ma) as the most well-studied OAEs. During both events, significant increases in oxygen are produced from the burial of reduced compounds, approximately 10–100% of modern atmospheric oxygen levels. The added LIP-reductants partially or even completely buffer this excess oxygen through the oxidation of reduced volatile compounds. Short-term increases in oxidative weathering show a similar magnitude of oxygen removal from the ocean-atmosphere system. This analysis highlights the importance of quantifying the oxygen budget during OAEs and similar events.

1. INTRODUCTION

Throughout Earth's history, there have been many intervals of widespread marine anoxia, with the most well-studied having occurred during the Mesozoic. These events reflect major disturbances to global climate and environment that lasted for several hundreds of thousands of years or longer (Jenkyns, 2010). They indicate geologically short-term departures from typical steady-state oxygen content of the ocean-atmosphere system, which is often assumed to be a balancing of various known processes (Holland, 2002). Oceanic anoxic events (OAEs) are specifically defined as intervals of increased black shale deposition across mul-

tipale basins indicating widespread impact of geochemical changes to the ocean (Schlanger & Jenkyns, 1976). Therefore, one of the defining features of these events is the accumulation of organic-rich sediments across large portions of the ocean during these intervals (Jenkyns, 2010; Kemp et al., 2022; Owens et al., 2018; Schlanger & Jenkyns, 1976), as well as perturbations to various geochemical cycles, most notably those of carbon and sulfur, but also other redox-sensitive elements (Gill et al., 2011; Jenkyns, 2010; Owens et al., 2013, 2018; Them, Gill, Caruthers, et al., 2017). Many of these OAEs had important effects on life at the time, with some coinciding with major extinction intervals (Bond & Grasby, 2017; Jenkyns, 2010). Thus, studying

^a Corresponding author: snewby@hku.hk

these events can better relate Earth system processes to dynamic intervals of faunal turnover.

Constraining and quantifying the mechanisms that allow for these long-term intervals of enhanced organic matter burial and reducing marine conditions while maintaining near-modern atmospheric oxygen (O_2) contents has been greatly understudied. The primary cause for these events is often related to warming of the atmosphere and/or ocean system, leading to enhanced nutrient runoff from a heightened hydrologic cycle and weathering intensity (Gernon et al., 2024; Meyer & Kump, 2008). It has been proposed that the enhanced flux of nutrients increased the rates of marine primary productivity, whereby subsequent respiration and remineralization of that organic matter consumed dissolved O_2 (Gernon et al., 2024; Jenkyns, 2010; Poulton et al., 2015). This may be compounded by reduced thermohaline circulation and lower retention of dissolved gases in warmer waters (Meyer & Kump, 2008). The depletion of O_2 across these intervals causes aerobic respiration rates to decrease until the consumption of organic matter was less than the supply, at which point, sedimentary organic matter burial rates increased. Additional factors, such as remineralization rates of organic matter increasing with temperature, cause some inconsistencies that make this broad relationship non-linear.

1.1. Reduced carbon and sulfur burial effects on oxygen

With respect to O_2 production, it has been shown through decades of work that the most important reduced compounds buried are species of carbon and sulfur (e.g., organic carbon, organic sulfur, and pyrite) (Berner, 2006; Berner & Canfield, 1989; Garrels & Lerman, 1981). The production and burial of these compounds require the release of O_2 as the product in the reaction (table 1). Since some organic carbon and pyrite sulfur are buried and sequestered from the system, they become unavailable for O_2 consumption, causing O_2 content of the ocean-atmosphere system to increase. Modeling efforts, such as GEOCARBSULF, have quantified the burial of carbon and sulfur as a means to document the long-term O_2 budget of the Earth's surface (Berner, 1991, 2006, 2009; Berner & Canfield, 1989; Berner & Kothavala, 2001). The GEOCARBSULF model (Berner, 2006) and prior GEOCARB model (Berner & Canfield, 1989) utilize the presence of organic carbon-rich rocks in the sedimentary record and the burial of pyrite, both interpreted through isotope work, to determine the amount of O_2 production from burial of reduced species entering the atmosphere through the Phanerozoic using bins of several million years (i.e., longer than short-term OAEs). These calculated O_2 contents are modulated by many different mechanisms, but are mainly calculated using global marine carbon and sulfur isotope compositions to estimate the burial of organic carbon and pyrite sulfur (Berner, 2006; Berner & Canfield, 1989; Berner & Kothavala, 2001).

Similar studies have focused on the potential of carbon and sulfur burial to increase O_2 across the Great Oxidation Event and Lomagundi carbon isotope excursion (CIE), the Neoproterozoic Oxygenation Event and Shuram CIE, and

the Cambrian rise in O_2 (Bristow & Kennedy, 2008; Eguchi et al., 2020; Miyazaki et al., 2018; Saltzman et al., 2011). Other models utilize similar concepts with other variables, evidence and datasets, such as the COPSE model (Bergman et al., 2004). These studies have suggested that the burial of vast quantities of reduced carbon and sulfur induced O_2 production and global oxygenation, yet Phanerozoic anoxic events also buried copious amounts of these compounds but instead are associated with deoxygenation. Thus, there is disconnect for these shorter timescale events. Notably, the burial of carbon and sulfur has also been linked to changes in phosphorus cycling due to this element being a major bioessential nutrient (Van Cappellen & Ingall, 1994), and such changes have been modeled to show notable fluctuations corresponding with important carbon cycle perturbations that relate to these increases in O_2 (Bergman et al., 2004; Reershemius & Planavsky, 2021; Reinhard & Planavsky, 2022).

This quantitative approximation through modeling is a similar process to what is implemented across Mesozoic OAEs, where carbon and sulfur geochemistry is utilized to estimate the burial of their respective reduced species (Gill et al., 2011; Jenkyns, 2010; Kemp et al., 2022; Owens et al., 2013, 2018; Ruebsam & Schwark, 2024; Them et al., 2022), yet the O_2 production that such burial would cause are often under-discussed in favor of just quantifying this burial solely as an effect of widespread anoxia during such multi-millennial events due to proxy sensitivity (e.g., Dickson et al., 2017; Gill et al., 2011; Owens et al., 2013, 2018; Them, Gill, Caruthers, et al., 2017). Therefore, the burial of reduced chemical species should be investigated as a negative feedback mechanism that should cause O_2 production during the development of an OAE. This re-oxygenation feedback should occur on the tens of thousands of year timescale such that OAEs should be self-limiting in duration (Reershemius & Planavsky, 2021).

There are a variety of other phenomena that could extend the duration of OAEs, such as reactivity rates of organic carbon and pyrite sulfur formation, changes to ocean mixing times, stratification of seawater, or localized development of anoxia, both temporally and spatially. All of these would increase the duration of OAEs from durations of typical ocean-atmosphere circulation (~1,000 to 6,000 years), but not to the order magnitudes suggested by the geologic record. If other processes slow the rate of O_2 release from the burial of reduced species, it could limit this reoxygenation until after the OAE due to atmospheric oxygen response time being longer than the event itself. Subsequently, the excess O_2 could result in measurable and resolvable changes in various ocean-atmospheric processes and biologic impacts following the event. There is no evidence from the sedimentary record to support this; instead, evidence for concurrent increases in wildfire across the Toarcian OAE and Cretaceous OAE-2 suggest that O_2 may have been higher in the atmosphere during but not following the events (S. J. Baker et al., 2017; Boudinot & Sepúlveda, 2020). Additionally, other evidence suggests low oxygen conditions in marine bottom waters persisted long after these events rather than oxygenation (Ostrander et

Table 1. Chemical reactions related to the production or consumption of O₂ during OAEs

	General Reaction	Reaction Equation*	Stoichiometric O ₂ generation
O ₂ Production	Organic carbon burial	$\text{H}_2\text{O} + \text{CO}_2 = \text{CH}_2\text{O} + \text{O}_2$	1.00
	Pyrite sulfur burial	$2\text{Fe}^{2+} + 4\text{SO}_4^{2-} + 4\text{H}^+ = 2\text{FeS}_2 + 7\text{O}_2 + 2\text{H}_2\text{O}$	3.50
O ₂ Consumption	Hydrogen oxidation	$2\text{H}_2 + \text{O}_2 = 2\text{H}_2\text{O}$	-0.50
	Ammonia oxidation	$\text{NH}_3 + 2\text{O}_2 = \text{NO}_3^- + \text{H}^+ + \text{H}_2\text{O}$	-2.00
	Fe ²⁺ oxidation	$4\text{Fe}^{2+} + \text{O}_2 + 4\text{H}^+ = 4\text{Fe}^{3+} + 2\text{H}_2\text{O}$	-0.25
	Mn ²⁺ oxidation	$2\text{Mn}^{2+} + \text{O}_2 + 2\text{H}_2\text{O} = 2\text{MnO}_2 + 4\text{H}^+$	-0.50
	Hydrogen sulfide oxidation	$2\text{H}_2\text{S} + 2\text{O}_2 = \text{SO}_4^{2-} + 2\text{H}^+$	-1.00
	Methane oxidation	$\text{CH}_4 + 2\text{O}_2 = \text{CO}_2 + 2\text{H}_2\text{O}$	-2.00

*Bolding of important compound and O₂ for each reaction, with these on the product side of the equation for production and reactant side of the equation for consumption

al., 2017; Them et al., 2018). Therefore, the temporal extent of these events and lack of oxygen accumulation post-event (Bond & Grasby, 2017; Jenkyns, 2010) indicates additional processes must have occurred to sustain deoxygenation.

1.2. Mechanisms to reduce excess oxygen

The emplacement of large igneous provinces (LIPs) often coincide with OAEs and provide causal mechanisms for these global-scale marine deoxygenation intervals (Bond & Grasby, 2017; Green et al., 2022; Jiang et al., 2023; Kasbohm et al., 2021). LIPs supply a significant flux of mantle-derived carbon, primarily CO₂ (Bond & Grasby, 2017; Burgess et al., 2015; Fendley et al., 2024; Kasbohm et al., 2021), to the atmosphere, causing the climatic shifts likely needed to induce these events. This is often compounded by thermogenic carbon released from contact metamorphism of sedimentary rocks by the igneous intrusions (Chang et al., 2022; Flögel et al., 2011; Heimdal et al., 2021; Them, Gill, Caruthers, et al., 2017) or other feedbacks (e.g., wildfires, methane release from clathrate or wetlands) that also introduce carbon into the atmosphere from other sources (S. J. Baker et al., 2017; Boudinot & Sepúlveda, 2020; Huang et al., 2024; Them, Gill, Caruthers, et al., 2017). Additionally, other LIP-sourced materials, such as SO₂, aerosols, and particulates, may also induce major climatic changes, though these primarily induce short-term cooling (Bond & Grasby, 2017; Kasbohm et al., 2021).

This volatile-induced climate change has been a primary focus for research on the OAE-LIP relationship, but these volcanic provinces also likely introduced a variety of other reduced materials, such as iron (Fe²⁺), manganese (Mn²⁺), hydrogen sulfide (H₂S), hydrogen (H₂), methane (CH₄), and ammonia (NH₃) to the exogenic Earth during their emplacement (Edmonds et al., 2022; Sinton & Duncan, 1997). Such reducing species would react with available O₂, thereby removing it from the ocean-atmosphere system (table 1). There is additional evidence reducing volcanic emissions help counterbalance global redox changes from the formation of organic matter to some degree in the modern (Holland, 2002). However, limits on our knowledge of

the size and timing of eruptive activity as well as volatile composition, make it difficult to quantify the flux of reductants that LIPs could have been introduced to the system.

While size and timing of LIPs remain major focus of study, (Jiang et al., 2023; Kasbohm et al., 2021), their volatile chemistry remains comparatively understudied (Capriolo et al., 2021). Though not perfectly comparable to the subaerial LIPs that are the focus of this study, volatile flux estimates from modern hydrothermal systems at seafloor spreading centers were utilized here to approximate those from LIPs (Kasbohm et al., 2021; Mason et al., 2021). Other modern systems, namely mantle-plume-derived systems, suggested to be the most appropriate modern analog to LIPs, were also explored as LIP volatile analogs (Ilyinskaya et al., 2021; Jones et al., 2016; Mason et al., 2021; Self et al., 2008). However, differences in their volume and the areal extent of emissions compared to LIPs (most of these measurements are limited to singular vents), lack of data for some reduced compounds, and resulting flux estimations that ranged several orders of magnitude meant flux estimates from these systems were not utilized in this study (supplemental discussion). Further, work on emission from mantle-plume-derived systems (Campbell, 2005), suggest they are more similar to mid-oceanic ridge systems in terms of the redox potential of their emissions when compared to less reduced volcanic arcs systems (Holland, 2002). Overall, this indicates the assumption to utilize modern hydrothermal fluxes as analogs for LIP emissions is a reasonable approach.

That being said, there are certainly differences between mid-ocean ridge and subaerial LIPs systems (e.g., the infiltration of fluids into continental versus marine rocks and sediments) that may induce additional chemical changes that we do not account for here (Burgess et al., 2017; Green et al., 2022). However, even with the potential large uncertainties in estimating LIP reductant loads, the timing of the main phase(s) of LIP activity is often still well-correlated to time-equivalent OAEs, and many of their emplacements last as long as, if not longer than, their associated OAE (Bond & Grasby, 2017; Jiang et al., 2023; Kasbohm et al., 2021). Therefore, the LIPs likely still released significant

amounts of reduced compounds over the duration of these OAEs and must be considered when quantifying their global redox budgets.

An additional source of O_2 consumption is from oxidative weathering and is considered in both the GEOCARB and GEOCARBSULF models (Berner, 2001, 2006; Berner & Canfield, 1989; Berner & Kothavala, 2001). There is evidence for increased chemical weathering across many OAEs and is likely related to higher global temperatures and an enhanced hydrologic cycle (Frija & Parente, 2008; Kemp et al., 2020; McArthur et al., 2000; Percival et al., 2016; Pogge von Strandmann et al., 2013; Them, Gill, Selby, et al., 2017). Though chemical silicate weathering intensities do not directly relate to oxidative weathering, enhancement in silicate weathering is likely to correspond to increased oxidative weathering nonlinearly due to increases in physical weathering and enhanced hydrologic cycle effectively exposing fresh material to the oxygenated atmosphere (Berner, 2006; Berner & Kothavala, 2001; Daines et al., 2017; Gabet & Mudd, 2009). However, this nonlinear aspect is further compounded by the difference in oxidative weathering rate of reduced species, where sulfide minerals (e.g., pyrite) tend to oxidize more rapidly than organic matter during oxidative weathering (Littke et al., 1991; Petsch et al., 2000). In addition, there is a greater likelihood that younger, more labile reduced compounds are more rapidly oxidized, compared to longer-buried, more recalcitrant ones (Berner, 2006). This indicates that the age of exposed material is relevant but has limited applicability on the temporal scales that are the focus of this study (maximum of 10 million years) compared to long-term O_2 budget studies that involve more tectonic processes, which have bins around 10 million years (Berner, 2006, 2009). Thus, the relationship between silicate weathering intensity and oxidative weathering intensity is hard to quantify due to nonlinear interactions. However, a simplified relationship coupled with large and varied sensitivity tests in the model can give rough ranges for the effect of oxidative weathering on excess O_2 contents similar to approximations provided by the GEOCARBSULF model (Berner & Kothavala, 2001).

To analyze the net change in O_2 and potential chemical relationship between LIPs, oxidative weathering, and the redox evolution across OAEs, we focused on two of the most heavily studied OAEs, Oceanic Anoxic Event 2 (OAE-2, ~94 Ma) in the Cretaceous (Cenomanian-Turonian stage transition) and the Toarcian Oceanic Anoxic Event (T-OAE, ~184 Ma) in the Early Jurassic (post-Pliensbachian-Toarcian boundary). Both events have been primarily defined in recent work by their major associated CIEs as a chemostratigraphic markers (fig. 1A–B) and intervals of the widespread deposition of organic-rich sediments (Beerling & Brentnall, 2007; Bond & Grasby, 2017; Boulila et al., 2014; Dickson et al., 2017; Erbacher et al., 2005; Gill et al., 2011; Jenkyns, 1988; Y.-X. Li et al., 2017; Owens et al., 2013; Them, Gill, Caruthers, et al., 2017), but also supplementarily dated with biostratigraphic markers (Boulila et al., 2014; Corbett et al., 2014; Elder, 1989; Morten & Twitchett, 2009). Mass balance and forward box models were used to determine the O_2 produced via organic carbon and pyrite sulfur burial

compared to its consumption from the reductants released from the respective LIPs and oxidative weathering. Both O_2 consumption mechanisms, LIP reductants and oxidative weathering, were considered in isolation to determine their net effect on oceanic O_2 . Previous models of carbonate carbon isotopic variation across OAE-2 (Owens et al., 2013) and estimates of total organic carbon burial for the T-OAE (Them et al., 2022) along with carbonate-associated sulfate (CAS) sulfur isotopes for both events (Gill et al., 2011; Owens et al., 2013) were used to determine the organic carbon and pyrite sulfur buried, respectively (fig. 1C–D). The combination of O_2 production and O_2 consumption models presented here are a broad attempt to better constrain the O_2 budgets during OAEs beyond previous work with its limitations and assumptions discussed below.

1.3. Oceanic Anoxic Event 2

The record of the OAE-2 has been identified as the appearance of organic-rich sediments in various Upper Cretaceous sedimentary successions globally (Boudinot & Sepúlveda, 2020; Eldrett et al., 2015; Erbacher et al., 2005; Jenkyns, 2010; Meyers et al., 2012; Owens et al., 2018; Raven et al., 2019). This event also has a distinct positive CIE and positive sulfur isotope excursion associated with it (Dickson et al., 2017; Eldrett et al., 2015; Erbacher et al., 2005; Owens et al., 2013). These two features most likely indicate the enhanced burial of organic carbon and pyrite sulfur, respectively, on a globally relevant scale (Owens et al., 2013; Raven et al., 2019). The positive CIE is often used to define the duration event itself, and the interval containing it is associated with indicators of relatively warmer global temperatures (Bond & Grasby, 2017; Erbacher et al., 2005; Owens et al., 2013, 2018), increased silicate weathering (Frija & Parente, 2008; Pogge von Strandmann et al., 2013; Poulton et al., 2015), enhanced nutrient runoff from the continents (Y.-X. Li et al., 2022; Poulton et al., 2015), expansion of seafloor anoxia (Clarkson et al., 2018; S. Li et al., 2023; Montoya-Pino et al., 2010; Ostrander et al., 2017), and elevated rates of extinction, albeit only marginally greater than background rates (Bond & Grasby, 2017; Cocconi & Galeotti, 2003; Elder, 1989). The wealth of available geochemical information has been the subject of numerous investigations, especially the carbon and sulfur cycles across the event, making it an ideal interval of study to determine the potential increases in O_2 production due to the burial of reduced species.

One of the difficult challenges for understanding the drivers of OAE-2 is the number and variety of LIPs that have been invoked with this event. This is primarily due to poor age constraints for the associated LIPs. The Ontong Java LIP, Kerguelen LIP, Madagascar LIP, Caribbean Plateau LIP, and High Arctic LIP (HALIP) have all been suggested to coincide with OAE-2 (Jiang et al., 2023; Kasbohm et al., 2021; Maher, 2001; Sinton & Duncan, 1997). Nevertheless, many studies suggest that the Caribbean Plateau LIP (97 to 80 Ma), located in the modern-day Caribbean Sea, is the primary driver due to the radiometric dates of this submarine LIP closely aligning with the timing of OAE-2 and its large spatial extent (Jiang et al., 2023; Kasbohm et al.,

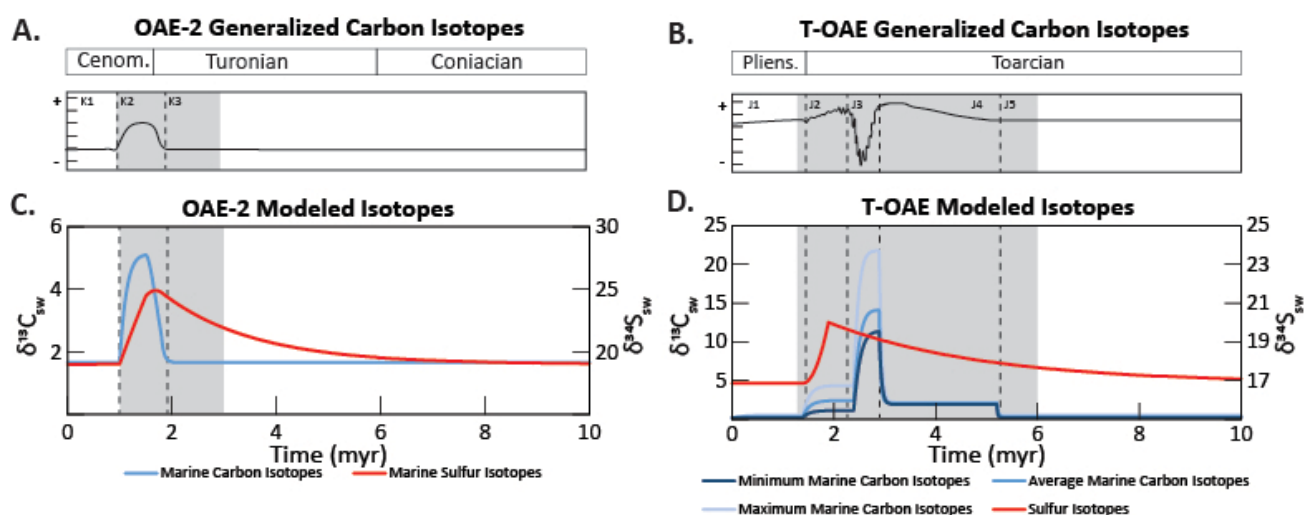


Figure 1. Idealized carbon isotopes and previously modeled carbon and sulfur isotopes of OAE-2 (A, C) and the T-OAE (B, D). (A) Idealized carbonate carbon isotopes of OAE-2 (Dickson et al., 2017; Erbacher et al., 2005), divided up into pre-CIE (K1), syn-positive CIE (K2), and post-CIE (K3). (B) Idealized carbonate carbon isotopes of the T-OAE (Them et al., 2022), divided up into Pliensbachian (J1), pre-CIE (J2), syn-negative CIE (J3), post-CIE (J4), and return to baseline (J5). (C) Modeled carbon and sulfur isotopic excursions of OAE-2 from previous work (Owens et al., 2013, 2018). (D) Modeled sulfur isotopic excursion from previous work on the T-OAE (Gill et al., 2011) and new modeled carbon isotopic excursion based on carbon burial data implied by Mo/TOC for the T-OAE (Them et al., 2022), excluding sources of ^{13}C -depleted carbon that would induce the observed negative CIE. Grey boxes represent approximate timing of main phase LIP activity for the respective OAE. Cenom. = Cenomanian, Pliens. = Pliensbachian.

2021). HALIP (93 to 89 Ma), a partially subaerial LIP located primarily in the Arctic Ocean and on several surrounding landmasses, also has a coeval date with OAE-2 (Jiang et al., 2023; Maher, 2001). Its major eruptive interval approximately spans 2 million years (Myr), and HALIP currently covers an area of approximately 200,000 km² (Kasbohm et al., 2021; Maher, 2001). Better spatial constraints and radiometric dating of this LIP (Jiang et al., 2023; Maher, 2001), as well as evidence of weathering of atmospherically exposed basaltic material (Pogge von Strandmann et al., 2013; Sullivan et al., 2020), make HALIP potentially a more suitable target for this study's models. Additionally, other continental LIPs are better associated with known global environmental perturbations throughout Earth History while few marine LIPs are (Green et al., 2022). This suggests that HALIP may have also been a greater contributor to this event.

Due to the limited dates on the LIP material, various scenarios of LIP activity were considered, including one based on the marine osmium records (Sullivan et al., 2020). This latter option includes three phases of volcanism that may have occurred during the early stages of OAE-2 (Y.-X. Li et al., 2022; Sullivan et al., 2020). Still, there is a lack of direct correlation between this proxy evidence of LIP activity and precise radiometric dating of HALIP volcanic deposits. The osmium isotope record also suggests significantly shorter volcanic activity than most estimates for the duration of HALIP and/or the other LIPs that have been associated with OAE-2 (Jiang et al., 2023; Kasbohm et al., 2021), and is therefore likely a conservative estimate for LIP activity.

Given this uncertainty, various other modeling scenarios for LIP eruptions were included in our scenarios for OAE-2.

Various proxies have been applied to the record of OAE-2 to constrain chemical silicate weathering rates and intensities. Osmium, lithium, and strontium isotopes proxies have all been applied to this OAE to approximate changes in silicate weathering and indicate a major increase in chemical weathering during the event (Frijia & Parente, 2008; Pogge von Strandmann et al., 2013; Poulton et al., 2015; Sullivan et al., 2020). The increases in silicate weathering have been linked to increased temperatures and hydrologic cycle activity (Gernon et al., 2024; Pogge von Strandmann et al., 2013; Poulton et al., 2015). Therefore, the estimated, model-derived 2 to 3 times increase in silicate weathering intensities across 200 thousand years (kyr) during OAE-2, which can provide an overall weathering rate increase for this interval, was utilized and likely had an impact on the oxidative weathering that could be incorporated into the model (Pogge von Strandmann et al., 2013).

1.4. Toarcian Oceanic Anoxic Event

The Early Jurassic T-OAE has also been identified from widespread organic matter-rich deposition at localities around the world (Cohen et al., 2004; Jenkyns, 1988, 2010; Kemp et al., 2022; Pálffy & Smith, 2000; Ruebsam et al., 2022; Ruebsam & Schwark, 2024; Them, Gill, Caruthers, et al., 2017). There is a noted CIE associated with this event, but it is a major negative excursion (~4–6‰) that likely represents greater input of isotopically light carbon to the ocean-atmosphere system (Beerling & Brentnall, 2007;

Bond & Grasby, 2017; Fendley et al., 2024; Gambacorta et al., 2024; Heimdal et al., 2021; Hesselbo et al., 2007; Jenkyns, 2010; Kemp et al., 2020; Ruebsam & Schwark, 2024; Them, Gill, Caruthers, et al., 2017). However, this negative CIE does not imply a lack of enhanced organic carbon burial during this event as evidenced by the occurrence of Toarcian organic-rich strata (Gambacorta et al., 2024; Kemp et al., 2022; Ruebsam et al., 2022; Ruebsam & Schwark, 2024). Further, a longer-term (3–4 Myr) positive CIE (~1–2‰) is found around the T-OAE, that is interrupted by the short-lived prominent negative CIE (Jenkyns, 2010; Them, Gill, Caruthers, et al., 2017) that has been interpreted to indicate enhanced carbon burial surrounding the T-OAE (Gambacorta et al., 2024; Jenkyns, 2010; Ruebsam & Schwark, 2024; Them et al., 2022; Them, Gill, Caruthers, et al., 2017). It, therefore, has been suggested that the positive carbon isotopic shift was transiently overwhelmed by the input of light carbon to induce a negative CIE (S. J. Baker et al., 2017; Ruebsam & Schwark, 2024; Them, Gill, Caruthers, et al., 2017).

Estimating organic carbon burial rates from this carbon isotope record is made complicated by the combined signals of the long-term positive and short-term negative CIEs. There has been much work focused on constraining the potential sources of ^{13}C -depleted carbon to the Earth system to account for this major negative CIE (S. J. Baker et al., 2017; Beerling & Brentnall, 2007; Huang et al., 2024; Kemp et al., 2020; Them, Gill, Caruthers, et al., 2017), but less emphasis on determining carbon burial and the budgets of the ocean-atmosphere O_2 . Other methods have to be employed to estimate organic carbon burial across the T-OAE either through globally mapping organic carbon contents of lithologies across this interval (Kemp et al., 2022; Ruebsam & Schwark, 2024) or comparing organic carbon content to other chemical proxies not affected by this pool of isotopically light carbon (Them et al., 2022). This latter method was employed due to the limited global mapping available (only around the Tethys) to provide sufficient model parameters (Kemp et al., 2022; Them et al., 2022).

Beyond this complication regarding the carbon isotope records, the T-OAE has many other well-constrained parameters that are useful for this study. There is a well-documented CAS sulfur isotope excursion that effectively estimates global pyrite burial (Gill et al., 2011). This interval, like OAE-2, is associated with rising global temperatures (Nordt et al., 2022), increased silicate weathering intensity (McArthur et al., 2000; Percival et al., 2015; Them, Gill, Selby, et al., 2017), enhanced nutrient runoff from the continents (Beerling & Brentnall, 2007; Kemp et al., 2020; Them, Gill, Selby, et al., 2017), expansion of seafloor anoxia (Gill et al., 2011; Them et al., 2018), and greatly elevated rates of extinction (Morten & Twitchett, 2009; Wignall et al., 2006, 2010), all of which are generally greater than equivalent changes for OAE-2.

What is well-constrained for the T-OAE is its strong temporal coincidence with the Karoo-Ferrar (K-F) LIP (185 to 181 Ma) (Burgess et al., 2015; Greber et al., 2020; Jiang et al., 2023; Kasbohm et al., 2021). This is one of the largest continental LIPs of the Phanerozoic (Jiang et al., 2023; Kas-

bohm et al., 2021), with a total surface area of 920,000 km^2 , separated into the Karoo province of Southern Africa and Ferrar province of Antarctica (Burgess et al., 2015; Kasbohm et al., 2021). Volcanic activity primarily spanned 4.5 Myr, though the major phases occurred over a smaller 300-kyr interval (Burgess et al., 2015; Greber et al., 2020).

In regard to weathering proxy records, there are less Toarcian records compared to OAE-2 and the primary proxy that has been applied in this regard is sedimentary osmium isotopes (Cohen et al., 2004; Kemp et al., 2020; Percival et al., 2016; Them, Gill, Selby, et al., 2017). There are potentially longer-term changes in weathering flux indicated in seawater strontium isotope record (McArthur et al., 2000), though these data do not aid with quantifying this flux during the shorter interval of the T-OAE due to strontium's longer residence time in the ocean. The osmium isotope data suggest a short-term (100 to 200 kyr) increase in silicate weathering intensity, 3 to 6 times greater than the modern intensities (Kemp et al., 2020), which again can be converted to average rate increase based on the known intensity and duration.

2. METHODS

2.1. Calculations for LIP reductant composition

To determine LIP reductant composition, data from modern hydrothermal activity of mid-oceanic ridges was utilized as an approximation. These were calculated by compiling the concentration of volatiles (in $\mu\text{mol/kg}$) from various hydrothermal systems (supplemental table 1). The volatiles that were included were Fe^{2+} , Mn^{2+} , H_2S , H_2 , CH_4 , and NH_3 (Charlou et al., 2000; Evans et al., 1988; Ishibashi et al., 2015; James et al., 2014; Ji et al., 2017; McDermott et al., 2018; Reeves et al., 2011; Seyfried et al., 2015; Von Damm, 1990) as previously utilized by earlier attempts to quantify O_2 reduction during OAEs (Sinton & Duncan, 1997). Due to the high variability in measured concentrations and various compounds having only limited data, the median concentrations were utilized for each compound. These were each then multiplied by the total global annual flux of hydrothermal material, an average of $7.2 \times 10^{12} \text{ kg/yr}$ (Nielsen et al., 2006), to result in a global flux for each compound (in mol/yr). Last, this was divided by the total global surface area of hydrothermal activity, $1.2 \times 10^{12} \text{ km}^2$ (E. T. Baker & German, 2004; Nielsen et al., 2006; Von Damm, 1990), to reach a reasonable approximation for the flux of each of these reductants per unit area. A similar methodology was attempted using island plume activity, mainly from Hawaii, but limitations in data and calculations proved this to be less useful (supplemental table 2). Due to the uncertainties of the comparability of LIP volatile fluxes to those of seafloor hydrothermal systems, this variable is modulated between half to double modern hydrothermal rates.

2.2. Forward Box Models for O_2 production

Forward geochemical box models were utilized for determination of net O_2 . These models assumed steady state of the O_2 budget prior to the event. Thus, the results from most

of the following equations and models are represented as changes from this steady state scenario rather than the actual abundances that may have existed in the ocean-atmosphere system, but these were also calculated through subtracting from the initial steady state values. For the production of O_2 from organic carbon and pyrite sulfur burial, box models of the carbon and sulfur cycles for OAE-2 (Owens et al., 2013) and the sulfur cycle for the T-OAE (Gill et al., 2011) were recreated (fig. 1). These used a time-dependent equation for the isotopic composition of the marine carbonate and sulfate reservoirs to reconstruct the marine isotope curves of these proxies. The following equation is for the time-dependent changes in marine carbonate carbon isotopes (a similar framework was applied to the sulfur cycle):

$$\frac{d\delta_{carb}}{dt} = \frac{\sum F_{in} (\delta_{in} - \delta_{sea}) - \sum F_{out} \Delta_{out}}{M_0}, \quad (1)$$

where δ_{carb} is the isotopic composition of the recorded values in carbonate (for the sulfur cycle this would be δ_{sulf}); δ_{sea} is the isotopic composition of the ocean at the time and is equivalent to δ_{carb} or δ_{sulf} ; F_{in} are the input fluxes to the ocean of the respective isotopic system being modeled in moles per year with an isotopic composition of δ_{in} ; F_{out} are the output fluxes from the ocean of the respective isotopic system being modeled in moles per year with an offset from seawater isotopic values of Δ_{out} , and M_0 is the initial amount of the respective element in the ocean reservoir in moles. For the carbon cycle, the only input is weathering, with the outputs being carbonate formation and organic carbon burial. See the later discussion for lack of including inputs of volcanogenic and thermogenic carbon. For sulfur, the inputs were weathering and hydrothermal fluxes and the outputs of sulfate and pyrite burial. For specific details on the initial parameters utilized and sensitivity tests to approximate isotopic curves found in the geologic record, see previous cited studies (Gill et al., 2011; Owens et al., 2013). For the purposes of this project, only the carbon burial rates and pyrite sulfur burial rates for the sensitivity tests thought to be most representative were utilized in our study for O_2 production during OAEs.

The organic carbon burial rates for the T-OAE utilized other studies based on molybdenum (Mo) to total organic carbon (TOC) ratios (Them et al., 2022) and a smaller estimate based primarily on an accounting of preserved organic-matter deposits formed during the event (Kemp et al., 2022). This new model attempts to recreate the T-OAE positive CIE based on organic carbon burial and not the major negative CIE likely caused by the large input of ^{13}C -depleted carbon from volcanism and other sources (Ruebsam & Schwark, 2024; Them, Gill, Caruthers, et al., 2017) using equation (1), as illustrated in figure 1B. Due to poorer constraints on organic carbon burial with the method utilized, the full range of estimated burial values from Them et al. (2022) and Kemp et al. (2022) were utilized for the model across the time interval studied instead of a single reasonable estimate for carbon burial rate as for OAE-2.

Stoichiometric calculations (table 1) were used to determine the amount of O_2 produced due to the burial of or-

ganic carbon and pyrite (table 2). This utilized the equation:

$$O_P(t) = 1 * (F_{org}(t) - F_{org}(0)) + 3.5 * (F_{py}(t) - F_{py}(0)). \quad (2)$$

where O_P is excess O_2 produced in moles; F_{org} is organic carbon burial in moles per year; $F_{org}(0)$ is initial organic carbon burial rate; F_{py} is pyrite burial in moles per year; and $F_{py}(0)$ is initial pyrite burial rate. The initial values, representative of baseline conditions prior to each event, were removed so that only excess O_2 production could be calculated rather than total O_2 production.

2.3. Forward Box Models for O_2 consumption

Additions to the forward geochemical box models were used to approximate the reducing components of the related LIPs, using the HALIP for OAE-2 (Kasbohm et al., 2021; Maher, 2001; Sinton & Duncan, 1997) and K-F LIP for the T-OAE (Burgess et al., 2015; Greber et al., 2020; Kasbohm et al., 2021). As there are relatively few estimates of the overall reductant load from these LIPs (Kasbohm et al., 2021; Sinton & Duncan, 1997), the reductant output of modern mid-oceanic ridge hydrothermal vent activity per surface area was utilized (supplemental table 1). Most recent estimates for duration and geographic extent of the LIPs were utilized for the modeled excursion of reductant material (Burgess et al., 2015; Kasbohm et al., 2021; Maher, 2001; Sinton & Duncan, 1997). These model parameters are in table 2. Variations on the extent of reductant output, aerial extent, duration, possible pulses of volcanism, weathering rates, and relation between silicate and oxidative weathering were modeled (table 3). Again, stoichiometric conversions were used to determine the amount of O_2 consumed due to the release of these reduced compounds (table 1). This results in the equation:

$$\begin{aligned} O_{CLIP}(t) &= A_{LIP}(t) * S_{LIP}(t) \\ &\quad * (0.25F_{Fe} + 0.5F_{Mn} + 1F_{H_2S} \\ &\quad + 2F_{CH_4} + 0.5F_{H_2} + 1.25F_{NH_3}), \end{aligned} \quad (3)$$

where O_{CLIP} is excess O_2 consumed by LIP reductants, A_{LIP} is the unitless scaling factor of LIP activity compared to modern hydrothermal activity (with 1 equivalent to modern hydrothermal reductant load per unit area per time), S_{LIP} is the surface area of active LIP in km^2 , and F_x represents the fluxes of various compounds derived from volcanic and hydrothermal activity in moles per km^2 per year. For the surface area of the LIPs, HALIP was assumed to be 200,000 km^2 for OAE-2 (Kasbohm et al., 2021; Maher, 2001) and the K-F LIP was modulated between 350,000 km^2 and 920,000 km^2 based on the specifically active province and the timing of active phases (Burgess et al., 2015; Greber et al., 2020; Jiang et al., 2023; Kasbohm et al., 2021). If the values of fluxes for modern hydrothermal activity (supplemental table 1) are included directly into equation (3), it can be simplified to create:

$$\begin{aligned} O_{CLIP}(t) &= (6.24 \times 10^{12} mol Myr^{-1} km^{-2}) \\ &\quad * A_{LIP}(t) * S_{LIP}(t). \end{aligned} \quad (4)$$

As thermogenic CH_4 has often been invoked as a major contributor to the climatic shifts at these times and is re-

Table 2. Initial model parameters for OAE-2 and T-OAE O₂ production and consumption

Initial Parameters	Variable (if available)	Values for OAE-2	Values for T-OAE
Marine Carbon Reservoir	M _{CO}	3.3 × 10 ¹⁸ mol	6.6 × 10 ¹⁸ mol
Carbon Weathering Flux	F _{Cin(w)}	25.015 × 10 ¹⁸ mol/Myr	50.000 × 10 ¹⁸ mol/Myr
Organic Carbon Burial	F _{org}	5.014 × 10 ¹⁸ mol/Myr	1.460 × 10 ¹⁸ mol/Myr
Marine Sulfur Reservoir	M _S	3.16 × 10 ¹⁸ mol	5.0 × 10 ¹⁸ mol
Sulfur Weathering Flux	F _{Cin(w)}	0.980 × 10 ¹⁸ mol/Myr	1.500 × 10 ¹⁸ mol/Myr
Sulfate Burial Flux	F _{py}	0.830 × 10 ¹⁸ mol/Myr	0.380 × 10 ¹⁸ mol/Myr
Carbon to Oxygen Production Rate	From table 1	1	1
Sulfur to Oxygen Production Rate	From table 1	3.5	3.5
LIP Reductants Oxygen Consumption Rate	ΣF _{red}	6.24 × 10 ¹² mol/km ² /Myr	6.24 × 10 ¹² mol/km ² /Myr
Silicate Weathering Rate	R _{cw}	1	1
Weathering Relation	r	1.5	1.5
Initial Oxidative Weathering	F _{owc} + F _{ows}	6.88 × 10 ¹⁸ mol/Myr	6.88 × 10 ¹⁸ mol/Myr

Table 3. Modeled Variables for OAE-2 and T-OAE

Variable	Range of Values	Notes
OAE-2		
LIP activity	0–2	1 is modern hydrothermal activity (M.H.)
Number of eruptive phases	0–4	
Duration of eruptive phases	0.1–2 Myr	Some dependence on number of phases
Amount of CH ₄ emission	1.13–3×10 ¹¹ mol/Myr/km ²	
Silicate weathering rate	1–3	1 is modern rate
Weathering relation	0.67–2	1.5 as used for GEOCARB
T-OAE		
Organic matter burial background rate	0.39–3.24×10 ¹⁸ mol/yr	From 0 to 1.39 Ma and 5.20 to 10 Ma
Organic matter burial Early Toarcian	0.39–9.97×10 ¹⁸ mol/yr	From 1.39 to 2.39 Ma
Organic matter burial during negative CIE	1.83–22.40×10 ¹⁸ mol/yr	From 2.39 to 2.89 Ma
Organic matter burial post-negative CIE	0.39–12.82×10 ¹⁸ mol/yr	From 2.89 to 5.20 Ma
LIP activity	0–2	1 is modern hydrothermal activity (M.H.)
Amount of CH ₄ emission	1.13–1.56×10 ¹¹ mol/Myr/km ²	
Silicate weathering rate	1–6	1 is modern rate
Silicate Weathering Duration	0.1–0.2 Myr	
Weathering Duration	0.67–2	1.5 as used for GEOCARB

lated during the emplacement of LIPs (S. J. Baker et al., 2017; Chang et al., 2022; Fendley et al., 2024; Heimdal et al., 2021), this parameter was varied for these events, increasing up to 3.00 × 10⁵ mol/yr/km² to account for potentially greater variability, and this change will slightly affect the flux term in equation (4).

To estimate oxidative weathering rates, the relationship from GEOCARB and GEOCARBSULF was utilized (Berner & Kothavala, 2001). It quantifies the relationship between silicate weathering rates and erosion rates as:

$$R_w = k * (R_e)^{2/3}, \quad (5)$$

where R_w is the weathering rate (specifically, silicate weathering), k is a constant, and R_e is the erosion rate (Berner & Kothavala, 2001). Assuming changes in erosional

rates are directly related to oxidative weathering rates and that removing the k constant will not change the proportional difference between oxidative weathering and erosion when the modern rates of both are known, a new equation was created:

$$F_{ow}(t) = (F_{owc} + F_{ows}) * R_{cw}(t)^r, \quad (6)$$

where F_{ow} is the effective oxidative weathering rate, F_{owc} and F_{ows} are the modern oxidative weathering rates of carbon and sulfur, respectively, R_{cw} is the effective chemical silicate weathering rate compared to modern (assuming current relative weathering rate is 1), and r is the weathering relationship between silicate weathering and oxidative weathering. The r variable is initially set to 1.5 as prescribed by the GEOCARB and GEOCARBSULF models

(Berner, 2006; Berner & Kothavala, 2001) since this relationship is inverted from equation (5) and is changed to a variable in order to explore this poorly constrained relationship. This variable is intended to cover the variety of potential uncertainties when comparing oxidative weathering to silicate weathering, including differences in weathering intensity of different compounds of different ages as well as other factors that lead to non-linear interactions between the two weathering types.

Since the modern oxidative weathering rates of organic carbon and pyrite sulfur have been estimated, 2.33×10^{12} and 0.83×10^{12} mol/yr, respectively (Burke et al., 2018; Daines et al., 2017), these can be substituted into the equation when combined with the oxygen consumption stoichiometry of organic carbon and pyrite sulfur (table 1). When introduced to the oxygen budget, the equation is:

$$O_{C_{weath}}(t) = (5.24 \times 10^{18} \text{ mol myr}^{-1}) * (R_{cw}(t)^r - 1), \quad (7)$$

where $O_{C_{weath}}$ is excess O_2 consumed by oxidative weathering and the initial value is subtracted to determine only excess oxygen consumption from oxidative weathering.

Both the LIP reductant and oxidative weathering were separately modeled and then combined to show changes in O_2 over time (figs. 2–6). This involved combining the outputs of equations (2) with equation (3) and/or (7), creating:

$$O_N(t) = O_P(t) - O_C(t), \quad (8)$$

where O_N is net O_2 . O_C was set to either O_{CLIP} (eq 3) or $O_{C_{weath}}$ (eq 7). Some scenarios were run with these together as a combined O_2 consumption ($O_C = O_{CLIP} + O_{C_{weath}}$). Net O_2 contents of all runs are displayed in supplemental tables 4 and 5. These values were further compared to determine the degree of O_2 removal as a percentage of the produced O_2 :

$$\%O_2 \text{ consumed} = \frac{O_C(t)}{O_P(t)}, \quad (9)$$

and these results are presented (supplemental discussion and supplemental figs. 2–6).

Each model run was conducted over a 10-million-year span to include the buildup and decline of the CIE, LIP activity, weathering rates, and all other pertinent phenomena related to these events. Iterations in inputs occurred every 5,000 years, with outputs every 1,000 years. Starting parameters (table 2) were incorporated across all iterations, while various other parameters were tested (table 3) in accordance with the specifics dependent on the OAE's available data and assumptions (supplemental tables 4–5).

3. RESULTS

A limited number of scenarios of O_2 production were modeled that focused on the sources of O_2 reduction (supplemental table 3). To this end, a variety of sensitivity tests were conducted that account for different scenarios that reduced the excess O_2 for both OAEs. Simplified results can be found in table 3, and a full list of each test done and pertinent results for the OAE-2 and T-OAE models can be found in supplemental tables 4 and 5, respectively.

3.1. OAE-2 model results

For OAE-2 (supplemental table 4), the total O_2 production from burial of reduced species remained the same across all runs. The net change in O_2 over time was calculated using information derived from the carbon and sulfur isotopic curves for OAE-2 (Owens et al., 2013). This interval is subdivided (fig. 1) into pre-CIE (K1, 1.00 Myr), syn-positive CIE (K2, 0.95 Myr), and post-CIE (K3, 8.05 Myr). There is an increase in excess O_2 produced during K2, releasing 3.73×10^{18} moles of O_2 across ~0.8 Myr (table 4, figs. 2,3), with similar amounts produced from both reduced carbon (2.04×10^{18} moles of O_2) and sulfur (1.69×10^{18} moles of O_2) burial (supplemental table 3).

Various models for the reductant emission loads from HALIP during OAE-2 were analyzed to determine the O_2 production, consumption, and net change (fig. 2, supplemental table 4). These covered a range of sizes, durations, and eruptive styles of the LIP (Kasbohm et al., 2021; Maher, 2001; Sinton & Duncan, 1997). Both continuous and pulsed intervals of volcanic activity were modeled (fig. 2A–D). Alternatively, osmium concentration and isotope indicators of volcanic activity around OAE-2 (Y.-X. Li et al., 2022; Sullivan et al., 2020) may represent pulses of LIP activity and this was also modeled (fig. 2E). A range of reducing material fluxes was considered for the LIP reductants compared to modern mid-oceanic ridge hydrothermal output (supplemental table 1). The abundance of thermogenic CH_4 was also modulated to determine the degree of impact this might have on the O_2 budget (fig. 2F), with minor effect ($<0.25 \times 10^{18}$ moles of O_2). Overall, the resulting models covered a broad range of net O_2 change across OAE-2, from -1.55×10^{18} moles of O_2 (net consumption) to 3.22×10^{18} moles of O_2 produced (table 4, fig. 2, supplemental table 4).

Another set of models was created to determine the effect of oxidative weathering on the O_2 consumption of OAE-2 (fig. 3, supplemental table 4). These primarily cover different rates of weathering, incorporating the silicate weathering rates and intensities of previous studies (Pogge von Strandmann et al., 2013) over 200 kyr (fig. 3A). Another series of sensitivity tests evaluated the effective exponent to describe the relationship between silicate weathering and oxidative weathering, deviating from the value utilized by Berner and Kothavala (2001) in the GEOCARB models from an exponential value of 1.5 (fig. 3B). Overall, the resulting models covered a similar range to the LIP reductants, from -3.47×10^{18} moles of O_2 (net consumption) to 2.57×10^{18} moles of O_2 produced (table 4, fig. 3, supplemental table 4).

3.2. T-OAE model results

A carbon model using a recently determined range of organic carbon burial for the T-OAE (Them et al., 2022) was created to determine the degree of O_2 production. The interval surrounding the T-OAE can be subdivided into separate time bins based on the carbon isotope curve, specifically the negative CIE, with labels J1 through J5 (fig. 1) utilized for all other figures and modeling. These bins divide the interval into late Pliensbachian (J1, 1.39 Myr),

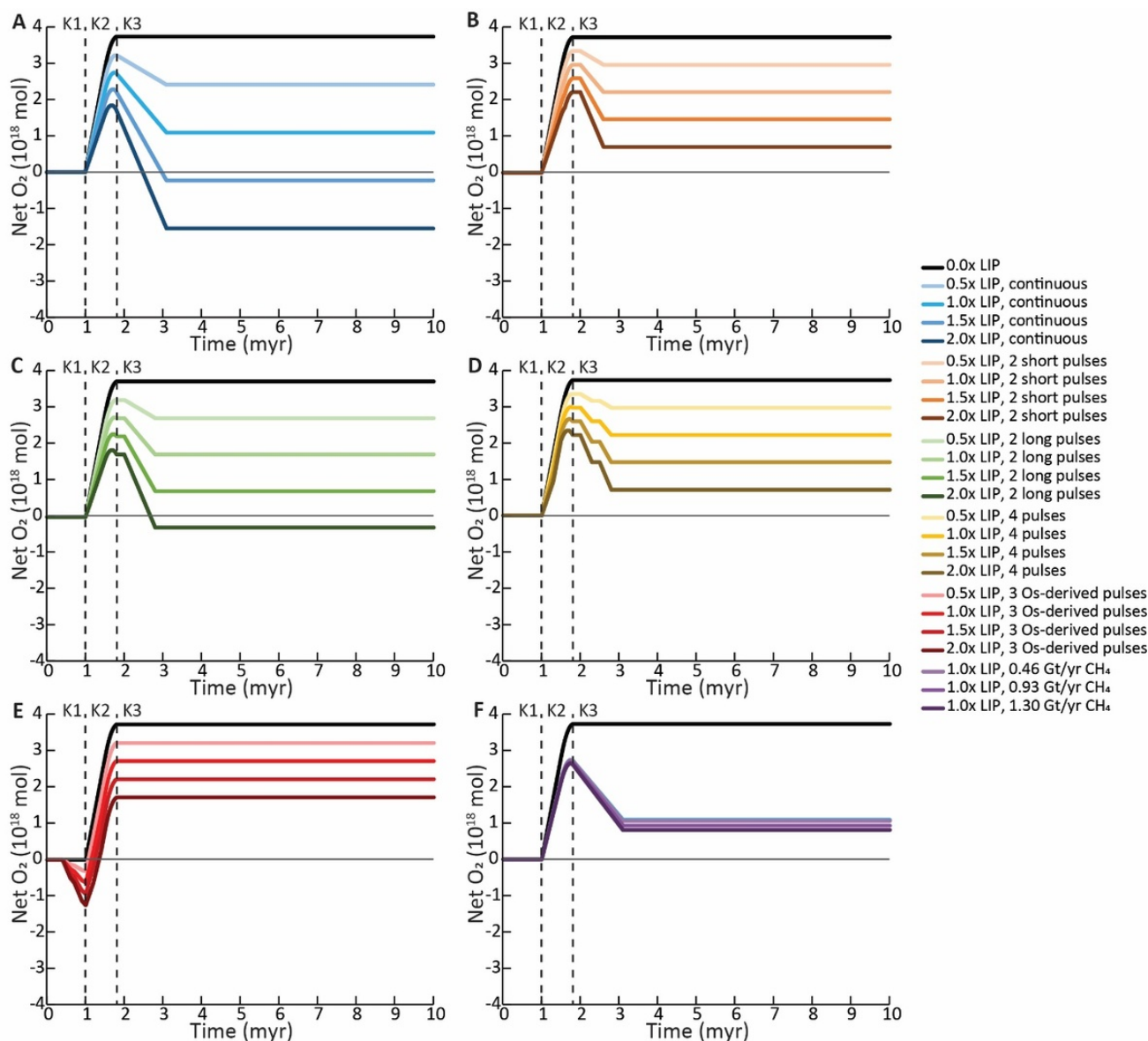


Figure 2. Net O₂ production based on buried organic carbon and pyrite sulfur compared to LIP reductant input for OAE-2 across various sensitivity tests. (A) Modeled continuous volcanism across 2 Myr starting at the onset of OAE-2 (K2) modulating the total reductant output. (B) Modeled impact of two pulses of volcanism, each lasting 500 kyr. (C) Modeled impact of two pulses of volcanism, each lasting 700 kyr. (D) Modeled impact of four pulses of volcanism, each lasting 200 kyr. (E) Modeled impact of three pulses of volcanism based on the timing of osmium excursions (Y.-X. Li et al., 2022; Sullivan et al., 2020). (F) Modeled impact of increased CH₄ release based on thermogenic carbon estimates (Chang et al., 2022) compared to the continuous run with 1.0× LIP activity (A), though the difference between this run and the 0.5× additional CH₄ makes them indistinguishable in figure. The 0.0× LIP model runs show the total O₂ produced via burial of reduced carbon and sulfur without additional reductants from LIP activity.

Toarcian pre-CIE (J2, 1.00 Myr), syn-negative CIE (J3, 0.50 Myr), post-CIE (J4, 2.31 Myr), and return to baseline (J5, 4.80 Myr). Utilizing recently published data of Mo/TOC to recreate organic carbon burial (27.4×10^{18} to 48.4×10^{18} moles of carbon buried) over the span of ~1.3 Myr (Them et al., 2022), a positive CIE is modeled with an excursion size of 11.4‰ to 21.8‰, averaging 13.6‰ (fig. 1D). All of these model runs produce a small positive CIE during J2, which increases the isotopic composition by about 0.9‰ to 4.3‰, followed by a major increase to the isotopic max-

imum during J3, then greatly decreasing to just slightly heavier values (1.7‰ to 2.2‰) than pre-event baseline in J4. At this point, a new positive isotopic plateau is maintained across J4 before returning to the original baseline of 0‰ at J5. Even if isotopically depleted carbon in volcanic CO₂ (~5‰) from K-F LIP is included in the model (Jones et al., 2016), the effect of this light volcanic carbon is so minute (<0.03‰) that it can only slightly negate the positive CIE produced (supplemental table 5). Thus, the carbon isotopic effect of LIP emissions is ignored for the purposes

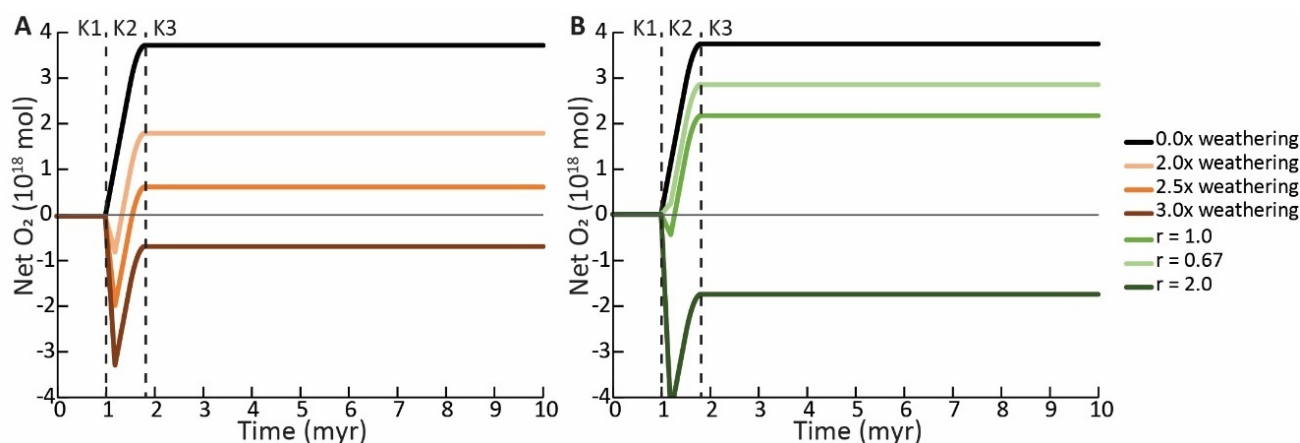


Figure 3. Net O₂ production based on buried organic carbon and pyrite sulfur compared to oxidative weathering for OAE-2 across various sensitivity tests. (A) Modeled increases in weathering (Pogge von Strandmann et al., 2013) at the onset of OAE-2 (K2). (B) Modeled impact of changing the ratio utilized for r (see Methods) from a baseline of 1.5 with the average weathering rate of 2.5 \times (Berner & Kothavala, 2001). The 0.0 \times weathering model runs show the total O₂ produced via burial of reduced carbon and sulfur without additional oxidative weathering.

of these newly derived excursions. An alternative model based on Kemp et al. (2022) was also utilized to estimate total organic carbon burial. These data only focus on the interval of the negative CIE, and therefore all changes were relegated to J3. This calculation provided much smaller estimates for organic carbon burial, which results in a much smaller positive CIE at this time (0.7‰).

We utilized the methods established for OAE-2 model (described above) with the constraints for the T-OAE (supplemental table 5) to create a model that estimated O₂ change over time using previous models for degree of pyrite sulfur burial for the T-OAE with a conservative, parsimonious estimate of 5×10^{17} moles (Gill et al., 2011). This resulted in a total of 1.58×10^{18} moles of O₂ production over 0.5 Myr (supplemental table 3). Conversely, the new T-OAE carbon model based on Them et al. (2022) suggests a very large range of O₂ production due to the wide range of quantities for possible organic carbon burial, with all models indicating a much greater O₂ production via organic carbon burial (20.64×10^{18} to 36.31×10^{18} moles O₂ produced) than that determined for pyrite burial (supplemental table 3). Over the course of the increased organic carbon burial interval, lasting ~ 3.3 Myr, between 22.2×10^{18} and 37.9×10^{18} moles of O₂, averaging 27.8×10^{18} moles of O₂, can be produced from the combined reduced sulfur and carbon burial (fig. 4–6). The model results using Kemp et al. (2022) provide a smaller production of O₂ than even OAE-2, totaling 2.30×10^{18} moles of O₂ (fig. 4D).

The various model estimates for the T-OAE organic carbon and pyrite sulfur burial were combined with modeled LIP activity based on previously published literature (Burgess et al., 2015; Greber et al., 2020; Kasbohm et al., 2021) to determine O₂ production and consumption and subsequently the overall net change. The LIP activity was varied (supplemental table 5) to account for potential variability in the reductant flux (supplemental table 1). An additional model utilizing the minimum organic carbon burial estimates (Them et al., 2022) was used to modulate the

effect of CH₄ inclusion on the oxidative budget of LIPs (fig. 4E), with minor effect ($<0.11 \times 10^{18}$ moles of O₂). Other tests for CH₄ were employed on the different carbon burial scenarios (supplemental table 5). The resulting models cover a broader range of net O₂ change across the T-OAE as compared to OAE-2, from -21.46×10^{18} moles of O₂ (net consumption) to 31.95×10^{18} moles of O₂ produced (table 4).

Another set of models were created to determine the effect of oxidative weathering on the O₂ budget of the T-OAE (fig. 5, supplemental table 5). These all use the minimum organic carbon burial flux of Them et al. (2022) as a baseline for comparison. These primarily cover different rates, intensities, and durations of weathering, incorporating the silicate weathering rates of previous studies (Them, Gill, Selby, et al., 2017) to estimate oxidative weathering (fig. 5A–C). Another series of sensitivity tests evaluated the effective exponent to describe the relationship between silicate weathering and oxidative weathering, deviating from the value utilized by Berner and Kothavala (2001) in the GEOCARB models from an exponential value of 1.5 (fig. 5D). Overall, the resulting models covered a smaller range than the LIP reductants, from 3.44×10^{18} to 19.35×10^{18} moles of net O₂ produced (table 4, fig. 5, supplemental table 5), partially due to limiting the modeling to a singular carbon burial scenario.

3.3. Combined Results

A final model set was employed for both OAEs combining the LIP reductant and oxidative weathering to determine the total degree of O₂ consumption that might be estimated from these processes. For OAE-2 various tests were employed to estimate the different LIP activity styles but utilized the average of oxidative weathering scenarios (supplemental table 4). This results in a complete utilization of O₂ across all scenarios, with net O₂ between -1.38 and -3.12×10^{18} moles of O₂ (table 4, fig. 6A, supplemental table 4).

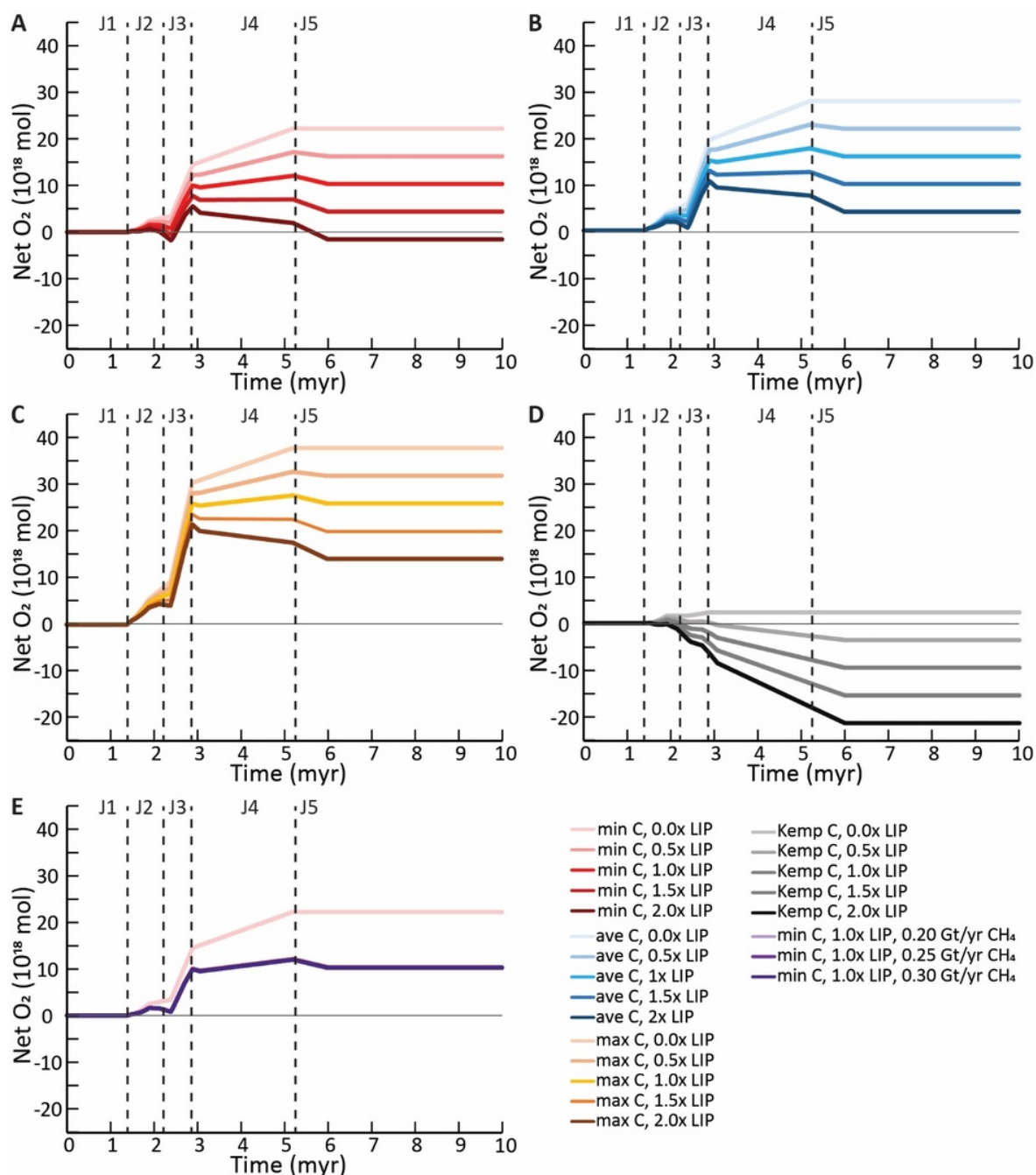


Figure 4. Net O_2 production based on buried organic carbon and pyrite sulfur compared to LIP reductant input for the T-OAE across various sensitivity tests for LIP activity. All panels use different amounts of organic carbon burial based on previous studies but the same pyrite sulfur burial rates (Gill et al., 2011). (A) Modeled O_2 produced and consumed under minimum carbon burial rates from Them et al. (2022). (B) Modeled O_2 produced and consumed under average carbon burial rates from Them et al. (2022). (C) Modeled O_2 produced and consumed under maximum carbon burial rates from Them et al. (2022). (D) Modeled O_2 produced and consumed using Kemp et al. (2022) estimates of global carbon burial. (E) Modeled O_2 produced and consumed under minimum carbon burial rates from Them et al. (2022), modulating CH_4 content while LIP activity is set to $1.0\times$ (Heimdal et al., 2021), though the additional CH_4 is indistinguishable in figure compared to $1.0\times$ LIP activity. The $0.0\times$ LIP model runs show the total O_2 produced via burial of reduced carbon and sulfur without additional reductants from LIP activity. min = minimum estimated organic carbon burial, avg = average estimated organic carbon burial, max = maximum estimated organic carbon burial.

For the T-OAE, various sensitivity tests were employed to examine the average LIP activity and oxidative weathering rate over different organic carbon burial regimes (sup-

plemental table 5). This results in heavy, though not always complete, utilization of O_2 across all scenarios, with a net

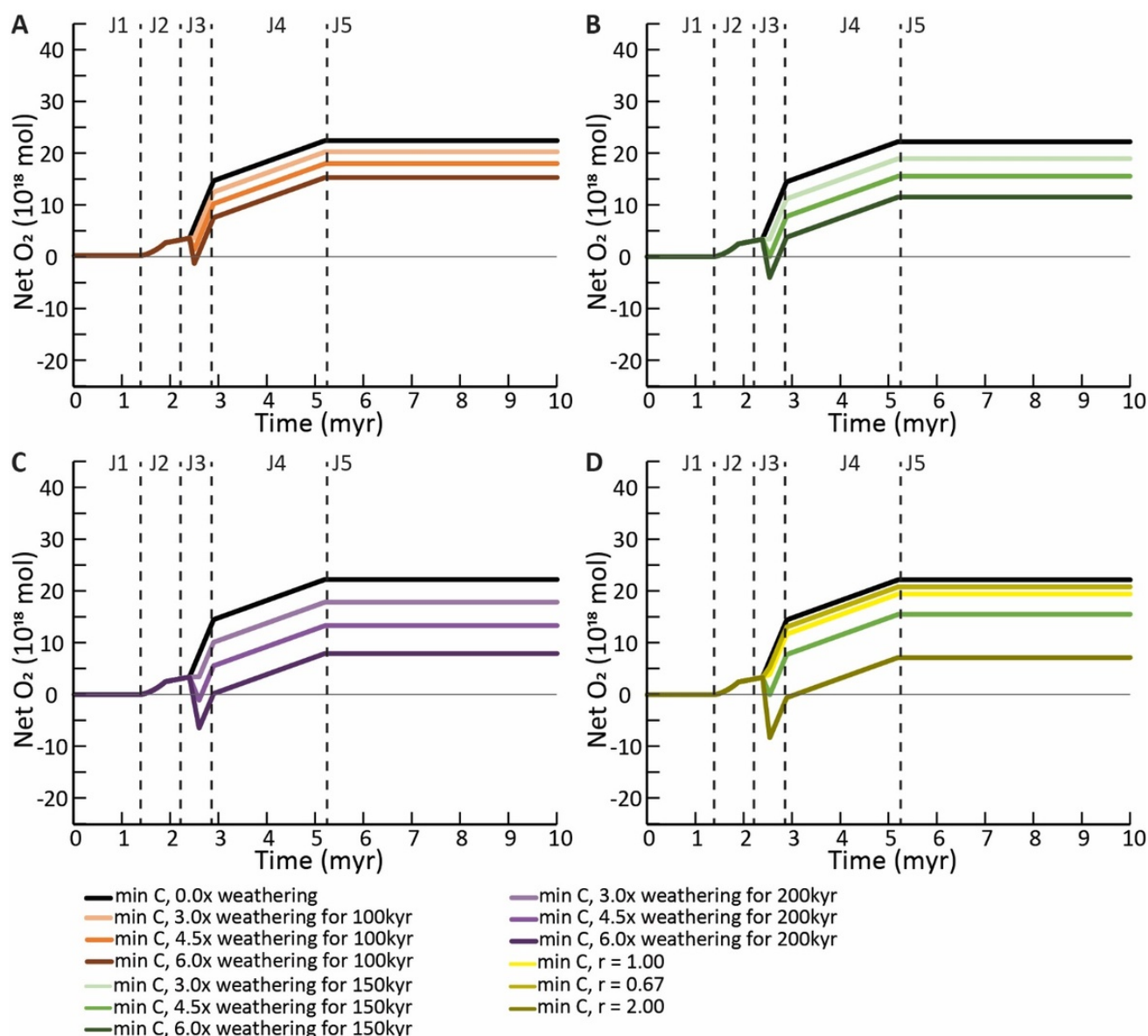


Figure 5. Net O₂ production based on buried organic carbon and pyrite sulfur compared to oxidative weathering for the T-OAE across various sensitivity tests. (A) Modeled increases in weathering (Them, Gill, Selby, et al., 2017) at the onset of the negative CIE (J3) for 100kyr. (B) Modeled increases in weathering (Them, Gill, Selby, et al., 2017) at the onset of the negative CIE (J3) for 150kyr. (C) Modeled increases in weathering (Them, Gill, Selby, et al., 2017) at the onset of the negative CIE (J3) for 200kyr. (D) Modeled impact of changing the ratio utilized for *r* (see Methods) from a baseline 1.5 with the average weathering rate and duration of 4.5x for 150kyr (Bernier & Kothavala, 2001). The 0.0x weathering model runs show the total O₂ produced via burial of reduced carbon and sulfur without additional oxidative weathering.

O₂ consumption and production between -18.46 and 17.12 × 10¹⁸ moles of O₂ (table 4, fig. 6B, supplemental table 5).

4. DISCUSSION

4.1. Assumptions for model creation

These models provide quantitative results, albeit with uncertainties due to ambiguity concerning the model inputs, that can be used as a guide for future investigations related to the fundamental operation of OAEs. However, several of these uncertainties in the presented work should be dis-

cussed further, including quantifying the role of the reductant fluxes from LIPs and the estimation of oxidative weathering rates. The production of O₂ due to reduced carbon and sulfur burial requires a simple stoichiometric calculation, but the exact amount of organic carbon and/or pyrite sulfur buried requires mass balance modeling, which is under-constrained for some of the parameters, resulting in multiple solutions. Several methods have been employed to determine the range of potential burial fluxes of reduced species utilizing inorganic carbon isotopes, organic carbon isotopes, global mapping of organic-rich sediments and their geochemical compositions, and other lithologic con-

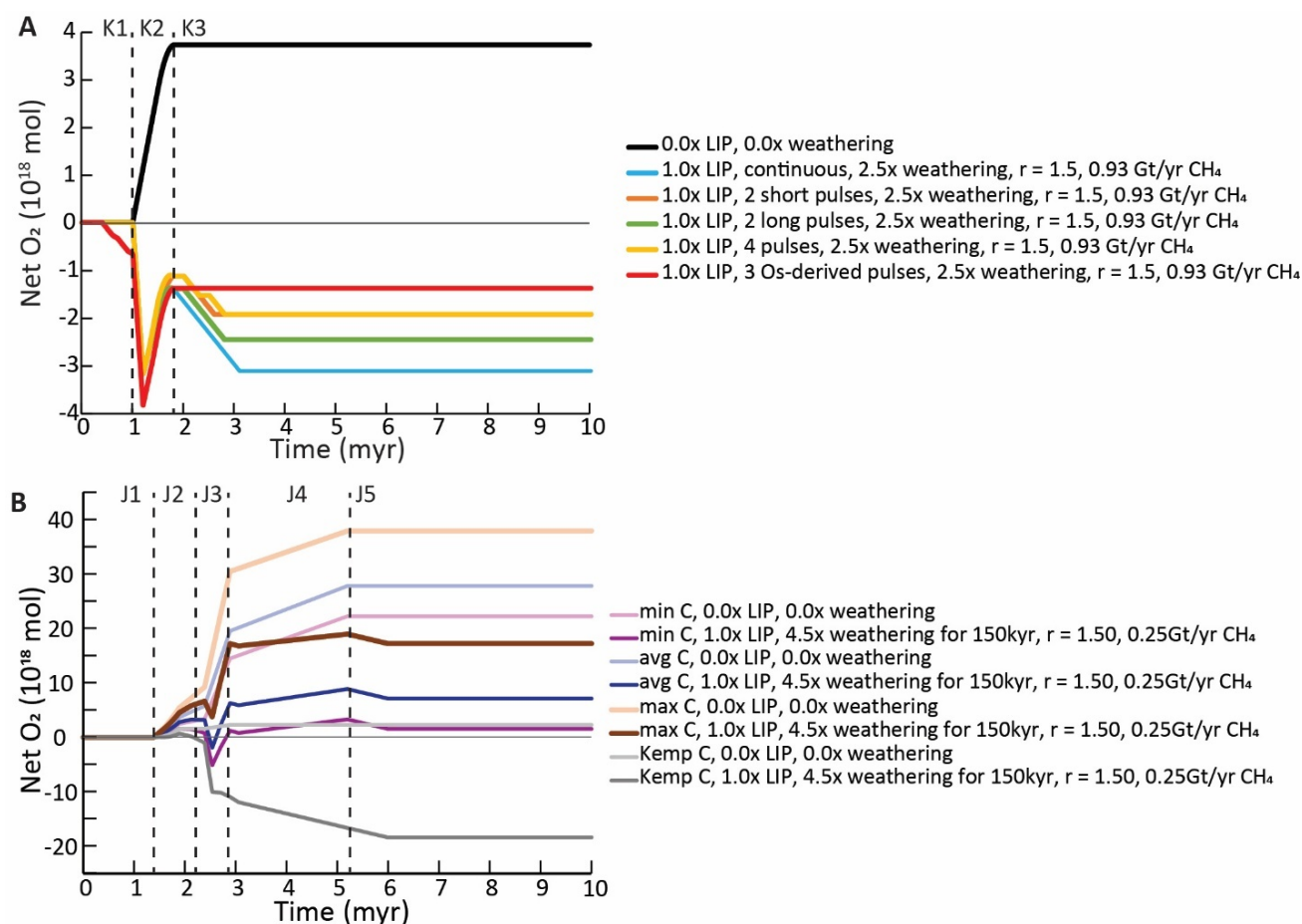


Figure 6. (A) Net O₂ production based on buried organic carbon and pyrite sulfur compared to a combination of baseline LIP activity models and oxidative weathering for OAE-2. (B) Net O₂ production based on the various buried organic carbon scenarios (Kemp et al., 2022; Them et al., 2022) and pyrite sulfur burial compared to a combination of baseline LIP activity models and oxidative weathering for the T-OAE.

Table 4. Summarized results of models for OAE-2 and the T-OAE

Model Set	O ₂ Produced (×10 ¹⁸ mol)	Net O ₂ (×10 ¹⁸ mol) (% removed*)		
		Maximum†	Median	Minimum†
OAE-2				
LIP	3.73	3.22 (14%)	1.72 (54%)	-1.55 (142%)
Weathering	3.73	2.57 (31%)	0.44 (88%)	-3.47 (545%)
Combined	3.73	-1.38 (137%)	-1.93 (152%)	-3.12 (184%)
T-OAE				
LIP (Kemp carbon burial)	2.30	-3.64 (258%)	-9.58 (517%)	-21.46 (1033%)
LIP (minimum carbon burial)	22.22	16.28 (27%)	10.34 (53%)	-1.54 (107%)
LIP (average carbon burial)	27.79	21.85 (21%)	15.91 (43%)	4.03 (85%)
LIP (maximum carbon burial)	37.89	31.95 (16%)	26.01 (31%)	14.12 (63%)
LIP (all)	25.01	31.95 (16%)	12.23 (50%)	-21.46 (1033%)
Weathering (minimum carbon burial)	22.22	20.44 (8%)	12.86 (42%)	2.49 (89%)
Combined	25.01 (median)	17.12 (55%)	4.25 (84%)	-18.46 (903%)

*Percent of the O₂ produced that is consumed under these scenarios

†The minimum and maximum are in terms of net O₂ amounts, with negative values representing O₂ consumption. Thus, the lower the net O₂ the more of an effect the process has.

straints (Erbacher et al., 2005; Gill et al., 2011; Kemp et al., 2022; Owens et al., 2013, 2018; Raven et al., 2019; Ruebsam et al., 2022; Them et al., 2022). The model presented here primarily incorporates isotopes from inorganic carbon and carbonate-associated sulfate sulfur isotope studies as they more quantifiably represent the burial of their respective reduced compounds at a global scale (Gill et al., 2011; Owens et al., 2013). However, for the flux of organic carbon burial during the T-OAE being more complicated we have utilized a study that incorporates Mo/TOC values because of the inherent limitations when working only with the carbon-isotope record – i.e., sources of light carbon inducing a negative CIE (Ruebsam & Schwark, 2024; Them et al., 2022). Previously determined estimates for reduced species burial used to recreate the respective isotope excursions (Gill et al., 2011; Owens et al., 2013) were used as a starting point for the models presented here (fig. 1), with the focus of this work being on the negative feedbacks that consume O₂. Organic sulfur could also represent a portion of the reduced sulfur burial during these OAEs that would change the absolute degree of O₂ production. However, organic sulfur burial is a poorly constrained during most Phanerozoic OAE intervals, and even those that recognize the potential importance organic sulfur have not quantified its global burial flux (Raven et al., 2019). Therefore, to simplify the models, all reduced sulfur is assumed to be pyrite as it is likely the dominant species, though additional sensitivity tests reveal limited effect from the replacement of pyrite with organic sulfur as a major sulfur species, at greatest ~25% less O₂ produced if all sulfur was buried as organic sulfur instead of pyrite (supplemental fig. 1).

To remedy the issue of a negative CIE during the T-OAE masking the carbon isotopic signal of increases in organic carbon burial, a novel calculation of organic carbon burial inferred from molybdenum geochemistry in organic-rich sediments was utilized (Them et al., 2022). Previous studies on this ratio were used to interpret global marine molybdenum concentration from better established organic carbon burial of OAE-2 (Owens et al., 2016), so the reverse was done for the T-OAE (Them et al., 2022). This provided several potential O₂ production scenarios from carbon burial for the T-OAE (fig. 2A) and the range of tests was done to account for the uncertainty in calculations using this methodology (Bernier, 2006; Bernier & Canfield, 1989; Owens et al., 2013, 2018). In addition, the estimated positive CIE that this organic carbon burial would have created (excluding input of ¹³C-depleted carbon; fig. 1D) would be greater than any previously documented for the Phanerozoic (Bond & Grasby, 2017; Cramer & Jarvis, 2020). It is possible that the magnitude of the carbon isotope excursion could be modulated by changing the isotopic fractionation of organic matter burial from seawater (Cui et al., 2021). However, a constant typical value of -25‰ was employed in the model for simplicity given the range of uncertainty (Owens et al., 2013). Since the exploration of the size of the positive CIE is not a primary focus of this study, this was not considered further. Nevertheless, emphasis should be put on the minimum organic carbon burial scenarios due to the uncertainty of these estimates.

The minimum organic carbon burial rate creates a large CIE (11.4‰) that places it a slightly larger than the largest Phanerozoic CIEs (< ~10‰) (Cramer & Jarvis, 2020). However, even this consideration means that the negative CIE that is recorded in the geologic record represents far greater input of isotopically light carbon than previous studies have suggested to compensate for the positive CIE that is produced by this buried organic carbon, as suggested by Them et al. (2022). If this Mo/TOC derived estimate for organic carbon burial is utilized there should be a degree of caution since these large CIEs are greater than other known positive carbon excursion of the Phanerozoic (Cramer & Jarvis, 2020). However, this still serves as starting point to compare with later O₂ consumption scenarios to evaluate the effect of the O₂ consumption mechanisms in our models. Therefore, while caution should be applied to this method for calculating global organic carbon burial, the broad trends in modeled T-OAE O₂ budgets are still likely representative but potentially at a higher absolute O₂ levels.

Conversely, an alternative concept for estimating organic carbon burial during the T-OAE utilized a global mapping technique of organic carbon mass accumulation rate of various sediments, primarily from European basins, and comparing that to excess methane carbon input that created the negative CIE fully converting to organic carbon buried (Kemp et al., 2022). The modeled carbon isotope excursion from this burial estimate created an ~0.7‰ positive CIE (supplemental table 5). However, it seems that these values significantly underestimate the total organic carbon burial during the T-OAE (Cohen et al., 2004; Jenkyns, 1988; Kemp et al., 2022; Ruebsam et al., 2022; Ruebsam & Schwark, 2024; Them, Gill, Caruthers, et al., 2017) and, therefore, are less likely to represent the amount of total O₂ production (supplemental discussion). Thus, the minimum carbon burial rate of Them et al. (2022) was the primary estimate used in this study while utilizing various other values in sensitivity tests (fig. 4B; supplemental table 5), especially those not involving LIP activity (fig. 5).

As mentioned above, there are a few uncertainties associated with the flux of materials from LIPs since there is no modern analog for these styles of eruptive events, even when not considering the volatiles released from the intruded country rock. Hotspot volcanism derived from mantle plumes may be most comparable due to having a similar source (Edmonds et al., 2022; Jones et al., 2016; Mason et al., 2021; Self et al., 2008). There are means to approximate the reducing volatile emission rate of hotspot magmatism by comparing the ratios of chemical species in modern emissions and using the better constrained portion of the ratios, such as Cl or SO₂, to determine the unknown half of the ratio, representing emitted compounds, and upscaling for LIP activity (Mason et al., 2021; Self et al., 2008). However, this method has uncertainties due to comparing volatiles to other volatiles, which may not be preserved in the geologic record. Nevertheless, estimates based on these were quantified (supplemental discussion, supplemental table 2) and found to be several orders of magnitude less than that from hydrothermal activity.

Therefore, mid-ocean ridge hydrothermal activity has been used as a preferred semi-analogous, first-order estimate for LIP reductants due to being a similarly mantle-derived source of material (Holland, 2002) while also having comparable magnitudes of spatial extent to OAE-like LIPs (supplemental table 1) with broad sensitivity tests on the direct relation to cover various possibilities (fig. 2). Thermogenic release of host rock volatiles from magmatic infiltration has been suggested to have contributed to biogeochemical changes across several recognized intervals and may have contributed to the reductant release of LIPs (Beerling & Brentnall, 2007; Burgess et al., 2017; Green et al., 2022; Jiang et al., 2023). Nevertheless, previous work has not quantified these volatiles for LIPs beyond potential methane (Beerling & Brentnall, 2007), thus the simplified mid-ocean ridge hydrothermal compositions are utilized here, but thermogenic volatiles should be considered in future work.

Another important mechanism for consumption of O_2 is oxidative weathering; however, there are many assumptions that must be made to approximate the effect when there is no current proxy available to accurately quantify global oxidative weathering rates under an oxygen-rich atmosphere. There are several studies that point to a relationship between physical erosion intensity and oxidative weathering intensity (Bernier & Kothavala, 2001; Daines et al., 2017; Gabet & Mudd, 2009; Riebe et al., 2003). These are mechanistically linked through the exposure of reduced species to oxidization by the atmosphere. However, the oxidation rate of different species, their age, as well as the degree of exposure necessary to induce oxidative weathering adds complexity this relationship. Additionally, there are no global scale proxies for physical erosion rates in deep-time to the quantifiable degrees needed for modeling exercises presented here (Bernier & Kothavala, 2001; Pogge von Strandmann et al., 2023). Changes in other proxies, such as temperature, may provide sufficient means to estimate changes in weathering, though these are unlikely to be directly related to the oxidative weathering changes due to their indirect relationships to the exposure of fresh rock material (Gernon et al., 2024). These also remain several steps removed from providing quantitative estimates of oxidative weathering rates.

Attempts to estimate ancient oxidative weathering for this study rely on the various proxies for silicate weathering (Misra & Froelich, 2012; Pogge von Strandmann et al., 2023) and signals from these proxies may not follow oxidative weathering processes (Kalderon-Asael et al., 2021; Lyons et al., 2014; Misra & Froelich, 2012; Reinhard et al., 2013). Specifically, this correlation is tenuous as there are various inconsistencies between silicate weathering and physical erosion (Daines et al., 2017; Gabet & Mudd, 2009; Pogge von Strandmann et al., 2023; Riebe et al., 2004) that would indicate changes in one may be incongruous with the other. However, many of the studies that have investigated these links focus on local weathering over shorter timespans (< 100 yrs) rather than geologic timescale variability.

When considering oxidative weathering on a global scale and over the long timescales, the GEOCARB model utilizes

a simplification of the relationship between silicate weathering and physical erosion (Bernier & Kothavala, 2001) that may provide a sufficient approximation. Nevertheless, the uncertain relationship between silicate and oxidative weathering leaves open uncertainties in how they can be related in terms of magnitude as well as their respective response time to other factors (physical erosion, climate, etc.). This includes lag in response time between rock exposure through erosion and subsequent chemical alteration by silicate weathering. The rate of the former is more pertinent to oxidative weathering though not a direct correlative while the latter is what can be approximated through proxy measurements. It is possible that the temperature increase that leads to enhanced silicate weathering can also induce hydrologic changes – e.g., enhanced rainfall and riverine flow – that can then induce increased exposure necessary for oxidative weathering, that is suggested to have occurred during the T-OAE (Them, Gill, Selby, et al., 2017). Additionally, there may be some difference in the response time between silicate and oxidative weathering due to differences in the oxidation rates of organic carbon and pyrite sulfur. While generally these rates are comparable on geologic time scales, processes during lithification can potentially change oxidation rate of rocks of different ages. Thus, in the presented modeling exercises various sensitivity tests were performed to provide a broad range of options for the effect of oxidative weathering, with silicate weathering proxies providing the best feasible quantitative estimates as a baseline for oxidative weathering rates.

4.2. Oxygen production across OAEs

The various assumptions and uncertainties used to create these models do not diminish the first-order implications of both the excess O_2 produced due to organic carbon and pyrite sulfur burial and/or the effect of various reducing mechanisms to consume excess O_2 . For OAE-2, we estimate that the total O_2 produced during the entire event through the burial of organic carbon and pyrite is 3.73×10^{18} moles (figs. 2,3,6), which is ~10% of modern atmospheric O_2 concentrations (36.4×10^{18} moles). This is a singular value for the produced O_2 across all OAE-2 models with the consumption of O_2 providing the control on the net O_2 due to only one set of organic carbon and pyrite sulfur burial rates being employed. The total O_2 produced by the T-OAE models is between 2.30×10^{18} and 37.89×10^{18} moles (figs. 4–6), with the most likely scenarios following the minimum carbon burial option of Them et al. (2022) that produced 22.22×10^{18} moles O_2 (fig. 4B). These values produce enough O_2 to be on the same size as modern atmospheric content (~60% to 100%). The production of O_2 during the T-OAE and even OAE-2 represent major imbalances in the ocean-atmosphere O_2 budget that must therefore be accounted for. Thus, some mechanism or mechanisms are necessary to limit the excesses accumulation of O_2 in order to maintain an OAE over their known million-year durations (Bond & Grasby, 2017; Jenkyns, 2010).

4.3. LIP impact on oxygen

We considered multiple scenarios of LIP eruptive styles for OAE-2 (Y.-X. Li et al., 2022; Sullivan et al., 2020), and these results are shown in [figure 2](#). The initial set ([fig. 2A](#)) includes continuous eruption for the approximate duration of HALIP, which generally induces the largest reductant-driven consumption of O_2 across the OAE-2 LIP reductant scenarios. There are also scenario sets for 2 eruptive pulses, for various durations, and 4 eruptive pulses to account for the uncertainty in the history of HALIP activity ([fig. 2B–D](#)). All of these scenarios induce less O_2 consumption compared to continuous eruption scenario. The models based on the osmium isotope record (Y.-X. Li et al., 2022; Sullivan et al., 2020) feature the lowest amount of O_2 removal from LIP reductants ([fig. 2E](#)) due to reduced inferred volcanic activity compared to the other scenarios, and these are likely conservative based on the uncertainties assigning specific pulses of volcanism to solely what the osmium isotope proxy records indicate. There are a few scenarios modeled that consume all the produced O_2 . This indicates that it is possible to completely remove all O_2 produced from the burial of reduced species simply through LIP activity, though this is unlikely as these are the end-members scenarios with the highest consumption fluxes. All other model runs show a major increase in the amount of O_2 consumed compared to not including LIP activity in the model. There is a consumption of between 0.51 and 5.28×10^{18} moles of O_2 , or 14% to 142% of the produced O_2 , through the oxidation of LIP reductants across the modeled scenarios ([fig. 2](#), supplemental fig. 2). Since these modeled sensitivity tests were not randomly selected, a true average is not possible to ascertain, but a median of the different sensitivity tests was determined to provide an approximation of average model output of 1.50×10^{18} moles, or 54%, of O_2 consumption ([table 4](#)). Overall, this reveals there was likely overall increase in net O_2 rather than a balance or loss across the event and therefore that there were likely additional processes beyond LIP activity that consumed O_2 .

A smaller set of eruptive scenarios was considered for the T-OAE due to the relatively well-constrained history of volcanism (Burgess et al., 2015; Greber et al., 2020; Kasbohm et al., 2021), only modulating the uncertainty in the amount of reductants released. Additional scenarios were also employed to account for the less-constrained range of carbon burial (supplemental table 5). Similar to OAE-2, all model runs for the T-OAE show significant O_2 consumption by LIP-derived reductants of the O_2 produced from the burial of reduced species. Across the model runs, between 5.94 and 23.76×10^{18} moles of O_2 were consumed, or 16% to 107% – up to 1033% for some of the models that utilize Kemp et al. (2022)'s lower estimates for carbon burial – of the produced O_2 ([fig. 4](#), supplemental fig. 4). Like OAE-2 model results, an average cannot be completely determined, but the median of these runs was 50% consumption across all the different burial scenarios ([table 4](#)). Similar to OAE-2, most of these model runs produced excess O_2 accumulation, but also a significant consumption of O_2 did occur. Therefore, also like the OAE-2 models, additional mechanisms are required to remove the excess O_2 from

the ocean-atmosphere system in order to maintain the observed duration of the OAE.

Across the model of both the T-OAE and OAE-2, the effect of CH_4 modulation was small. This species is often invoked as an important driver of climatic change from LIP activity, either as direct volcanic emission or released thermogenically during contact metamorphism of sedimentary rocks (S. J. Baker et al., 2017; Chang et al., 2022; Fendley et al., 2024; Heimdal et al., 2021). This is also one of the several reduced compounds utilized in the calculations ([table 1](#)), but CH_4 's importance to global environment change means that there are other constraints on it that could be incorporated. However, even with this importance, when greater proportions of CH_4 were incorporated into the model, only an additional 0.28×10^{18} moles of O_2 (7%) were consumed for OAE-2 in the highest flux scenario ([fig. 2F](#)). For the T-OAE, only 0.11×10^{18} moles of O_2 (1%) extra were consumed with the greatest flux of CH_4 ([fig. 4E](#)). Far greater quantities of CH_4 would need to be introduced to the ocean-atmosphere system to have a more quantitatively important impact on the O_2 budget than current estimates for CH_4 released during these events (S. J. Baker et al., 2017; Chang et al., 2022; Fendley et al., 2024; Heimdal et al., 2021).

4.4. Oxidative weathering impact on oxygen

A variety of scenarios were employed for both OAEs to determine the effect of oxidative weathering on the O_2 budget. For OAE-2, the intensity of weathering was modulated across 200 kyr at 2 to 3 times the modern intensity to match the intensity and duration of weathering across this interval as suggested by proxy records (Pogge von Strandmann et al., 2013). This assumes that the exponential relation between silicate and oxidative weathering is 1.5 (Berner & Kothavala, 2001). This results in between 2.52 and 5.77×10^{18} moles, or 68% to 155%, of O_2 consumption ([fig. 3A](#), supplemental fig. 3A), which is a similar to, though slightly higher than, the range from the LIP activity (median 4.06×10^{18} moles of O_2 , or 106%). The range and median indicate that the expected oxidative weathering on its own could potentially provide the full consumption of excess O_2 during OAE-2. This can be further tested by changing the relation between silicate and oxidative weathering from that used for the GEOCARBSULF models. In this regard, the exponential value of r (eqs 6–7) is modulated between 0.67 and 2 and was modeled with the average weathering intensity of 2.5 times modern intensity (Pogge von Strandmann et al., 2013). This causes a much larger range of effects, between 1.16 and 7.20×10^{18} moles of O_2 , equivalent to 31% to 193%, consumption ([fig. 3B](#), supplemental fig. 3B). Therefore, this relationship can have a greater effect on the O_2 budget, but the potential range from the weathering effect is large due to the uncertainties with implementing this parameter as noted above. Unlike the LIP activity, the majority of scenarios for oxidative weathering during OAE-2 can consume much of the produced excess O_2 (assuming an r value of at least 1.5 is reasonable).

The results for the T-OAE are relatively similar to those from the OAE-2 models. However, they cover a slightly

wider range of O_2 consumption scenarios due to longer durations and increases in weathering intensity: between 100 and 200 kyr with 3 to 6 times increased weathering intensities compared to modern weathering (Them, Gill, Selby, et al., 2017). This leaves a larger set of O_2 consumption solutions, between 2.87 and 18.78×10^{18} moles of O_2 , or 13% to 85% consumption (fig. 5A–C, supplemental fig. 5A–C), with a median of 13.44×10^{18} moles of O_2 consumed, or 40% consumption. Interestingly, unlike the OAE-2 models, the highest-end consumption still does not completely consume the O_2 produced likely due to the higher O_2 produced from organic carbon burial. Compared to the T-OAE results for LIP activity, the O_2 consumed from oxidative weathering generally falls into a similar range. Again, the exponential value (r in eqs 6–7) was modulated using the average scenario of 150 kyr at 4.5 times modern weathering intensity (Them, Gill, Selby, et al., 2017). This ended up ranging between 2.49 and 20.44×10^{18} moles of O_2 , 8% to 89%, consumption (fig. 5D, supplemental fig. 5D), once more indicating that the value for this factor can cause a greater impact than just changes in weathering rate. Furthermore, this mechanism has the potential to consume a large proportion of the excess O_2 produced by the event, but uncertainty in its parameterization point to the need for additional constraints to assess its role in the O_2 budget.

4.5. Comparing and Contrasting OAEs

There are several ways in which the models for these two events differ. The greatest distinction is the amount of O_2 produced and consumed during each event. Production and consumption of O_2 during OAE-2 is approximately an order of magnitude smaller than the T-OAE across nearly all model runs. The difference in production of O_2 can be directly attributed to the larger amount of organic carbon burial predicted for the T-OAE (Them et al., 2022). Smaller quantitative estimates have been suggested (Kemp et al., 2022) and were modeled (fig. 4A) but are likely to be underestimating the total carbon burial (see supplemental discussion). The disparity in carbon burial between the two events is to be expected as the estimated organic carbon to pyrite sulfur burial for the two events are significantly different, with OAE-2 having a C/S (carbon to sulfur ratio) value ranging between 2 and 12 (Hetzl et al., 2009), averaging 5.7 (Owens et al., 2013), while the T-OAE has a range of C/S value from 32 to 62 based on this study (supplemental discussion). This could indicate that there was also a difference in the degree of deoxygenation, with OAE-2's lower carbon to sulfur burial ratio indicating widespread euxinic (anoxic with water column sulfide) conditions, while the T-OAE's massive disparity in carbon to sulfur burial potentially indicating more widespread anoxia, but less extensive euxinia, or potentially increased anoxia and carbon burial in non-marine environments (Xu et al., 2017).

Additionally, the greater degree of O_2 production for the T-OAE would require a large removal of O_2 to counterbalance the redox budget and maintain widespread reducing marine conditions (Them et al., 2018, 2022). The larger K-F LIP (Burgess et al., 2015; Greber et al., 2020; Kasbohm et al., 2021) could provide such a supply of greater reduc-

ing compounds to the atmosphere and ocean (Kasbohm et al., 2021; Maher, 2001). The difference of magnitude in spatial extent between the smaller HALIP ($\sim 200,000 \text{ km}^2$) of the Cretaceous (Kasbohm et al., 2021; Maher, 2001) and the larger K-F LIP ($\sim 2,000,000 \text{ km}^2$) of the Jurassic (Burgess et al., 2015; Greber et al., 2020; Jiang et al., 2023; Kasbohm et al., 2021) is of approximately the same difference as the O_2 produced for each event, assuming similar durations of these LIPs based on the limited and less certain age constraints (Jiang et al., 2023; Kasbohm et al., 2021). This may imply a relationship between the size of the LIP, the LIP-induced climate perturbation, organic carbon and pyrite sulfur burial, the amount of O_2 produced, and the amount of O_2 consumed via reductant load through volcanic activity, as the difference in magnitude of all of these parameters had nearly equal impact for OAE-2 and T-OAE (Bond & Grasby, 2017; Gill et al., 2011; Jiang et al., 2023; Kasbohm et al., 2021; Owens et al., 2013; Pogge von Strandmann et al., 2013; Them, Gill, Selby, et al., 2017; Them et al., 2022). On the other hand, weathering intensities during the T-OAE are estimated to be significantly greater than those prescribed for OAE-2 (Pogge von Strandmann et al., 2013; Them, Gill, Selby, et al., 2017). This difference is not a full order of magnitude and is why the influence of oxidative weathering during the T-OAE is not as impactful ($\sim 42\%$ O_2 consumption) when compared to OAE-2 ($\sim 88\%$ O_2 consumption). This points to a potentially greater significance of the LIP reductants in the O_2 budget, at least for these two OAEs, though oxidative weathering and other processes should not be discounted.

It should also be noted that there is an order-of-magnitude difference in biological extinction/turnover that occurred during OAE-2 and the T-OAE. OAE-2 is associated with several minor extinctions, coined as turnover events by some, that were localized and affected specific, limited groups of organisms (Coccioni & Galeotti, 2003; Elder, 1989). Meanwhile, the T-OAE is associated with a major extinction event that affected various faunal groups globally (Bond & Grasby, 2017; Caruthers et al., 2013; Morten & Twitchett, 2009; Wignall et al., 2006, 2010). This difference in extinction rate between the two events would match closely to the scalar relationship between LIP size and changes in net O_2 . Therefore, these shifts in O_2 budget could be correlative to the size of extinction and such factors should also be considered when looking at other extinction events.

4.6. An additional parameter – Phosphorous cycling

Overall, these sensitivity tests suggest OAEs are prone to producing large quantities of O_2 through the burial of reduced compounds that are likely counterbalanced by LIP activity and oxidative weathering. Both processes under most scenarios consume enough O_2 to maintain deoxygenation (fig. 6). However, additional processes may also bear on the O_2 budgets of these events (supplemental discussion).

One notable factor to consider is changes in the cycling of phosphorus during OAEs which may also be able to extend the duration of deoxygenation and further decrease

the excess net O_2 . Specifically, phosphorous absorbed onto the surfaces of Fe-oxide minerals is released into seawater when these oxides are dissolved as anoxic conditions become prevalent. This provides an important flux of this bi-limiting nutrient to the water column that can stimulate primary productivity, which in turn may induce more O_2 production in the shorter term but lead to greater deoxygenation and additional Fe-oxide dissolution in the longer term (Gernon et al., 2024; Reershemius & Planavsky, 2021; Van Cappellen & Ingall, 1994). This positive feedback loop will then follow until there are insufficient Fe-oxides to dissolve or the extent of anoxia on the ocean floor reaches some maximum dictated by other processes. This feedback loop would work with the mechanisms proposed in this study to extend the duration of deoxygenation, especially if LIPs and/or weathering also provide additional sources of phosphorous. This phosphorous feedback requires large amounts of Fe-oxides initially present for the feedback cycles to persist for several hundred thousand years and tracking this process in the sedimentary record is difficult due to a lack of appropriate proxies. One source of physical evidence is the eventual accumulation of Mn-rich sediments in the oxic shallow waters near to these anoxic regions, often referred to as “bathtub rings” like found in the Black Sea (Force & Cannon, 1988). These Mn-rich sediments are likely the product of Fe-Mn-oxide dissolution under anoxic conditions, though their accumulation and preservation is discontinuous and therefore do not provide a quantitative estimate for Fe-oxide dissolution during OAEs (Gambacorta et al., 2024).

Chemical weathering may also enhance phosphorous delivery via the weathering of basaltic rocks (Gernon et al., 2024) linking LIP activity and oxidative weathering as a potential nutrient source in addition to their role as O_2 sink. Constraining and quantifying changes to these processes in the geologic past beyond modeling due to the limited proxies for phosphorous cycling (Gernon et al., 2024). Regardless, this work and previous studies show that the LIP-reductant load (Sinton & Duncan, 1997), enhanced oxidative weathering (Berner, 2006; Berner & Canfield, 1989; Berner & Kothavala, 2001), and/or phosphorous cycling (Gernon et al., 2024; Reershemius & Planavsky, 2021) certainly played a role in the O_2 budgets of these events.

5. CONCLUSIONS

We provide a novel modeling study of the production and consumption of O_2 across two Mesozoic oceanic anoxic events. The burial of organic carbon and pyrite sulfur across OAE-2 and the T-OAE could have produced large amounts O_2 that approached the modern content of the atmosphere. For both events, input of reduced chemical species from LIPs could provide enough reductive flux to consume much of the excess produced O_2 . Similarly, oxidative weathering can also consume a major portion of the produced O_2 . There is variability across all the modeled scenarios in how much O_2 could be consumed, with the two mechanisms combined typically consuming the majority of excess O_2 . This consumption of O_2 can provide a mechanism to help

explain the protracted duration of OAEs. It is possible, based on some of the scenarios, that these processes conspire to result in net loss of O_2 from the ocean atmosphere system. In that case, additional processes provide an important underlying mechanism for an OAE. However, more accurate quantification, timing and duration is required to better constrain this relationship.

The order-of-magnitude difference in O_2 production and consumption between OAE-2 and the T-OAE matches the magnitude difference between the size of their respective LIP and the extinction rates observed with these two events. There are many other factors and processes, such as climate and marine productivity, as well as other elemental cycles, that were likely affected by the O_2 budget of OAEs and exploring these are avenues of future study.

There are other Phanerozoic C and S cycle perturbations based on large isotopic excursions that are not known to be tied to LIP emplacement (Bond & Grasby, 2017; Cramer & Jarvis, 2020; Jenkyns, 2010), and thus, understanding the O_2 budgets of these events likely require invoking additional mechanisms to produce and limit O_2 . Further, there are intervals of LIP activity that have no significant oceanic anoxia associated with them (Jiang et al., 2023; Kasbohm et al., 2021). This dichotomy emphasizes oxidative weathering and/or other processes on the global O_2 budget are factors that need to be considered for these events and the effect of LIP source reductants should also not be overlooked. Sources of variability in the response of the ocean and atmosphere during these events are likely the result of the particular starting state of the ocean atmospheric system: the spatial or temporal variability of physical processes in the oceans, the climate, other biogeochemical mechanisms, etc. (Berner & Kothavala, 2001; Gernon et al., 2024; Reershemius & Planavsky, 2021). However, the reductants introduced by LIPs and effects of oxidative weathering should be considered when studying these events.

The models presented here provide a framework for understanding of the processes that should be involved, but this work highlights where more constraint is needed to improve our understanding these events. Better estimates of LIP reductant loads, through better estimates of the elemental budgets of LIPs or better analogs for the release of material across the spatial extents of igneous provinces, would aid in constraining their impacts on O_2 budgets. Identification of the LIP(s) responsible for OAE-2 and timelines for their eruptive activity would sharpen our estimates for O_2 consumption from igneous-source reductants. Conversely, our understanding of the O_2 budget of the T-OAE would benefit from an improved approximation of the event-driven organic carbon burial. Additionally, the quantification of oxidative weathering needs better overall constraints especially given our best weathering proxies relate to silicate weathering, which is likely not directly comparable. Lastly, the impact of the phosphorous and iron cycles and their feedbacks across OAEs need to be better tracked to determine their role in the O_2 budget. All this future work would not only improve the models needed to determine the redox budgets across these anoxic events, but also

constrain the mechanisms involved in the development and termination of OAEs more generally.

.....

Acknowledgments

This work was funded by grants from the National Science Foundation (EAR-2026926) to JDO and BCG, Alfred P. Sloan Foundation FG-2020-13552 (JDO), and the FSU EOAS Winchester Fund for graduate student support (SMN). We greatly appreciate the contributions and suggestions from our two reviewers and the associate editor.

Author Contributions

SMN was the primary author and created the models utilized in this study. BCG and JDO provided portions of models from previous studies to be utilized. TRT contributed additional data sets to approximate important missing pa-

rameters. BCG, JDO, SAY, SMN, and TRT all provided insights and parameterizations for the models and contributed to editing of the text. JDO, BCG, and SMN all contributed some funding for the project.

Conflicts of Interest

The authors declare no conflict of interest.

Supplementary Data

<https://doi.org/10.17632/vgt7hjmnr.1>

Editor: C. Page Chamberlain, Associate Editor: Jonathan L. Payne

Submitted: October 21, 2024 EDT. Accepted: June 23, 2025 EDT. Published: September 11, 2025 EDT.



This is an open-access article distributed under the terms of the Creative Commons Attribution 4.0 International License (CCBY-4.0). View this license's legal deed at <http://creativecommons.org/licenses/by/4.0> and legal code at <http://creativecommons.org/licenses/by/4.0/legalcode> for more information.

REFERENCES

- Baker, E. T., & German, C. R. (2004). On the global distribution of hydrothermal vent fields. In C. R. German, J. Lin, & L. M. Parson (Eds.), *Mid-Ocean Ridges: Hydrothermal Interactions Between the Lithosphere and Oceans, Geophysical Monograph Series 148* (pp. 245–266). American Geophysical Union. <https://doi.org/10.1029/148GM10>
- Baker, S. J., Hesselbo, S. P., Lenton, T. M., Duarte, L. V., & Belcher, C. M. (2017). Charcoal evidence that rising atmospheric oxygen terminated Early Jurassic ocean anoxia. *Nature Communications*, 8(1). <https://doi.org/10.1038/ncomms15018>
- Beerling, D. J., & Brentnall, S. J. (2007). Numerical evaluation of mechanisms driving Early Jurassic changes in global carbon cycling. *Geology*, 35(3), 247–250. <https://doi.org/10.1130/G23416A.1>
- Bergman, N. M., Lenton, T. M., & Watson, A. J. (2004). COPSE: A new model of biogeochemical cycling over phanerozoic time. *American Journal of Science*, 304(5), 397–437. <https://doi.org/10.2475/ajs.304.5.397>
- Berner, R. A. (1991). A model for atmospheric CO₂ over Phanerozoic time. *American Journal of Science*, 291(4), 339–376. <https://doi.org/10.2475/ajs.291.4.339>
- Berner, R. A. (2001). Modeling atmospheric O₂ over Phanerozoic time. *Geochimica et Cosmochimica Acta*, 65(5), 685–694. [https://doi.org/10.1016/S0016-7037\(00\)00572-X](https://doi.org/10.1016/S0016-7037(00)00572-X)
- Berner, R. A. (2006). GEOCARBSULF: A combined model for Phanerozoic atmospheric O₂ and CO₂. *Geochimica et Cosmochimica Acta*, 70(23), 5653–5664. <https://doi.org/10.1016/j.gca.2005.11.032>
- Berner, R. A. (2009). Phanerozoic atmospheric oxygen: new results using the geocarbsulf model. *American Journal of Science*, 309(7), 603–606. <https://doi.org/10.2475/07.2009.03>
- Berner, R. A., & Canfield, D. E. (1989). A new model for atmospheric oxygen over Phanerozoic time. *American Journal of Science*, 289(4), 333–361. <https://doi.org/10.2475/ajs.289.4.333>
- Berner, R. A., & Kothavala, Z. (2001). GEOCARB III; a revised model of atmospheric CO₂ over Phanerozoic time. *American Journal of Science*, 301(1), 182–204. <https://doi.org/10.2475/ajs.301.2.182>
- Bond, D. P. G., & Grasby, S. E. (2017). On the causes of mass extinctions. *Palaeogeography, Palaeoclimatology, Palaeoecology*, 478, 3–29. <https://doi.org/10.1016/j.palaeo.2016.11.005>
- Boudinot, F. G., & Sepúlveda, J. (2020). Marine organic carbon burial increased forest fire frequency during Oceanic Anoxic Event 2. *Nature Geoscience*, 13(10), 693–698. <https://doi.org/10.1038/s41561-020-0633-y>
- Boulila, S., Galbrun, B., Huret, E., Hinnov, L. A., Rouget, I., Gardin, S., & Bartolini, A. (2014). Astronomical calibration of the Toarcian Stage: Implications for sequence stratigraphy and duration of the early Toarcian OAE. *Earth and Planetary Science Letters*, 386, 98–111. <https://doi.org/10.1016/j.epsl.2013.10.047>
- Bristow, T. F., & Kennedy, M. J. (2008). Carbon isotope excursions and the oxidant budget of the Ediacaran atmosphere and ocean. *Geology*, 36(11), 863–866. <https://doi.org/10.1130/G24968A.1>
- Burgess, S. D., Bowring, S. A., Fleming, T. H., & Elliot, D. H. (2015). High-precision geochronology links the Ferrar large igneous province with early-Jurassic ocean anoxia and biotic crisis. *Earth and Planetary Science Letters*, 415, 90–99. <https://doi.org/10.1016/j.epsl.2015.01.037>
- Burgess, S. D., Muirhead, J. D., & Bowring, S. A. (2017). Initial pulse of Siberian Traps sills as the trigger of the end-Permian mass extinction. *Nature Communications*, 8(1), 164. <https://doi.org/10.1038/s41467-017-00083-9>
- Burke, A., Present, T. M., Paris, G., Rae, E. C. M., Sandilands, B. H., Gaillardet, J., Peucker-Ehrenbrink, B., Fischer, W. W., McClelland, J. W., Spencer, R. G. M., Voss, B. M., & Adkins, J. F. (2018). Sulfur isotopes in rivers: Insights into global weathering budgets, pyrite oxidation, and the modern sulfur cycle. *Earth and Planetary Science Letters*, 496, 168–177. <https://doi.org/10.1016/j.epsl.2018.05.022>
- Campbell, I. H. (2005). Large Igneous Provinces and the Mantle Plume Hypothesis. *Elements*, 1(5), 265–269. <https://doi.org/10.2113/gselements.1.5.265>
- Capriolo, M., Marzoli, A., Aradi, L. E., Ackerson, M. R., Bartoli, O., Callegaro, S., Dal Corso, J., Ernesto, M., Gouvêa Vasconcellos, E. M., De Min, A., Newton, R. J., & Szabó, C. (2021). Massive methane fluxing from magma–sediment interaction in the end-Triassic Central Atlantic Magmatic Province. *Nature Communications*, 12(1), 5534. <https://doi.org/10.1038/s41467-021-25510-w>

- Caruthers, A. H., Smith, P. L., & Gröcke, D. R. (2013). The Pliensbachian-Toarcian (Early Jurassic) extinction, a global multi-phased event. *Palaeogeography, Palaeoclimatology, Palaeoecology*, 386, 104–118. <https://doi.org/10.1016/j.palaeo.2013.05.010>
- Chang, B., Huang, J., Algeo, T. J., Pancost, R. D., Wan, X., Xue, Y., Jia, J., Wang, Z., Hu, J., Wang, J., Wang, S., Wu, J., & Xie, S. (2022). Episodic massive release of methane during the mid-Cretaceous greenhouse. *GSA Bulletin*, 134(11–12), 2958–2970. <https://doi.org/10.1130/B36169.1>
- Charlou, J. L., Donval, J. P., Douville, E., Jean-Baptiste, P., Radford-Knoery, J., Fouquet, Y., Dapigny, A., & Stievenard, M. (2000). Compared geochemical signatures and the evolution of Menez Gwen (37°50'N) and Lucky Strike (37°17'N) hydrothermal fluids, south of the Azores Triple Junction on the Mid-Atlantic Ridge. *Chemical Geology*, 171(1–2), 49–75. [https://doi.org/10.1016/S0009-2541\(00\)00244-8](https://doi.org/10.1016/S0009-2541(00)00244-8)
- Clarkson, M. O., Stirling, C. H., Jenkyns, H. C., Dickson, A. J., Porcelli, D., Moy, C. M., Pogge von Strandmann, P. A. E., Cooke, I. R., & Lenton, T. M. (2018). Uranium isotope evidence for two episodes of deoxygenation during Oceanic Anoxic Event 2. *Proceedings of the National Academy of Sciences of the United States of America*, 115(12), 2918–2923. <https://doi.org/10.1073/pnas.1715278115>
- Coccioni, R., & Galeotti, S. (2003). The mid-Cenomanian Event: Prelude to OAE 2. *Palaeogeography, Palaeoclimatology, Palaeoecology*, 190, 427–440. [https://doi.org/10.1016/S0031-0182\(02\)00617-X](https://doi.org/10.1016/S0031-0182(02)00617-X)
- Cohen, A. S., Coe, A. L., Harding, S. M., & Schwark, L. (2004). Osmium isotope evidence for the regulation of atmospheric CO₂ by continental weathering. *Geology*, 32(2), 157–160. <https://doi.org/10.1130/G20158.1>
- Corbett, M. J., Watkins, D. K., & Pospichal, J. J. (2014). A quantitative analysis of calcareous nannofossil bioevents of the Late Cretaceous (Late Cenomanian-Coniacian) Western Interior Seaway and their reliability in established zonation schemes. *Marine Micropaleontology*, 109, 30–45. <https://doi.org/10.1016/j.marmicro.2014.04.002>
- Cramer, B. D., & Jarvis, I. (2020). Carbon Isotope Stratigraphy. In *Geologic Time Scale 2020* (pp. 309–343). <https://doi.org/10.1016/b978-0-12-824360-2.00011-5>
- Cui, Y., Li, M., van Soelen, E. E., Peterse, F., & Kürschner, W. M. (2021). Massive and rapid predominantly volcanic CO₂ emission during the end-Permian mass extinction. *Proceedings of the National Academy of Sciences of the United States of America*, 118(37). <https://doi.org/10.1073/pnas.2014701118>
- Daines, S. J., Mills, B. J. W., & Lenton, T. M. (2017). Atmospheric oxygen regulation at low Proterozoic levels by incomplete oxidative weathering of sedimentary organic carbon. *Nature Communications*, 8(1), 14379. <https://doi.org/10.1038/ncomms14379>
- Dickson, A. J., Saker-Clark, M., Jenkyns, H. C., Bottini, C., Erba, E., Russo, F., Gorbatenko, O., Naafs, B. D. A., Pancost, R. D., Robinson, S. A., van den Boorn, S. H. J. M., & Idiz, E. (2017). A Southern Hemisphere record of global trace-metal drawdown and orbital modulation of organic-matter burial across the Cenomanian–Turonian boundary (Ocean Drilling Program Site 1138, Kerguelen Plateau). *Sedimentology*, 64(1), 186–203. <https://doi.org/10.1111/sed.12303>
- Edmonds, M., Mason, E., & Hogg, O. (2022). Volcanic Outgassing of Volatile Trace Metals. *Annual Review of Earth and Planetary Sciences*, 50(1), 79–98. <https://doi.org/10.1146/annurev-earth-070921-062047>
- Eguchi, J., Seales, J., & Dasgupta, R. (2020). Great Oxidation and Lomagundi events linked by deep cycling and enhanced degassing of carbon. *Nature Geoscience*, 13(1), 71–76. <https://doi.org/10.1038/s41561-019-0492-6>
- Elder, W. P. (1989). Molluscan extinction patterns across the Cenomanian–Turonian Stage boundary in the western interior of the United States. *Paleobiology*, 15(3), 299–320. <https://doi.org/10.1017/s0094837300009465>
- Eldrett, J. S., Ma, C., Bergman, S. C., Ozkan, A., Minisini, D., Lutz, B., Jactet, S.-J., Macaulay, C., & Kelly, A. E. (2015). Origin of limestone-marlstone cycles: Astronomic forcing of organic-rich sedimentary rocks from the Cenomanian to early Coniacian of the Cretaceous Western Interior Seaway, USA. *Earth and Planetary Science Letters*, 423, 98–113. <https://doi.org/10.1016/j.epsl.2015.04.026>
- Erbacher, J., Friedrich, O., Wilson, P. A., Birch, H., & Mutterlose, J. (2005). Stable organic carbon isotope stratigraphy across Oceanic Anoxic Event 2 of Demerara Rise, western tropical Atlantic. *Geochemistry, Geophysics, Geosystems*, 6(6), Q06010. <https://doi.org/10.1029/2004GC000850>

- Evans, W. C., White, L. D., & Rapp, J. B. (1988). Geochemistry of some gases in hydrothermal fluids from the southern Juan de Fuca Ridge. *Journal of Geophysical Research: Solid Earth*, 93(B12), 15305–15313. <https://doi.org/10.1029/JB093iB12p15305>
- Fendley, I. M., Frieling, J., Mather, T. A., Ruhl, M., Hesselbo, S. P., & Jenkyns, H. C. (2024). Early Jurassic large igneous province carbon emissions constrained by sedimentary mercury. *Nature Geoscience*, 17(3), 241–248. <https://doi.org/10.1038/s41561-024-01378-5>
- Flögel, S., Wallmann, K., Poulsen, C. J., Zhou, J., Oschlies, A., Voigt, S., & Kuhnt, W. (2011). Simulating the biogeochemical effects of volcanic CO₂ degassing on the oxygen-state of the deep ocean during the Cenomanian/Turonian Anoxic Event (OAE2). *Earth and Planetary Science Letters*, 305(3–4), 371–384. <https://doi.org/10.1016/j.epsl.2011.03.018>
- Force, E. R., & Cannon, W. F. (1988). Depositional model for shallow-marine manganese deposits around black shale basins. *Economic Geology*, 83(1), 93–117. <https://doi.org/10.2113/gsecongeo.83.1.93>
- Frijia, G., & Parente, M. (2008). Strontium isotope stratigraphy in the upper Cenomanian shallow-water carbonates of the southern Apennines: Short-term perturbations of marine ⁸⁷Sr/⁸⁶Sr during the oceanic anoxic event 2. *Palaeogeography, Palaeoclimatology, Palaeoecology*, 261(1–2), 15–29. <https://doi.org/10.1016/j.palaeo.2008.01.003>
- Gabet, E. J., & Mudd, S. M. (2009). A theoretical model coupling chemical weathering rates with denudation rates. *Geology*, 37(2), 151–154. <https://doi.org/10.1130/G25270A.1>
- Gambacorta, G., Brumsack, H. J., Jenkyns, H. C., & Erba, E. (2024). The early Toarcian Oceanic Anoxic Event (Jenkyns Event) in the Alpine-Mediterranean Tethys, north African margin, and north European epicontinental seaway. *Earth-Science Reviews*, 248, 104636. <https://doi.org/10.1016/j.earscirev.2023.104636>
- Garrels, R. M., & Lerman, A. (1981). Phanerozoic cycles of sedimentary carbon and sulfur. *Proceedings of the National Academy of Sciences*, 78(8), 4652–4656. <https://doi.org/10.1073/pnas.78.8.4652>
- Gernon, T. M., Mills, B. J. W., Hincks, T. K., Merdith, A. S., Alcott, L. J., Rohling, E. J., & Palmer, M. R. (2024). Solid Earth forcing of Mesozoic oceanic anoxic events. *Nature Geoscience*, 17(9), 926–935. <https://doi.org/10.1038/s41561-024-01496-0>
- Gill, B. C., Lyons, T. W., & Jenkyns, H. C. (2011). A global perturbation to the sulfur cycle during the Toarcian Oceanic Anoxic Event. *Earth and Planetary Science Letters*, 312(3–4), 484–496. <https://doi.org/10.1016/j.epsl.2011.10.030>
- Greber, N. D., Davies, J. H. F. L., Gaynor, S. P., Jourdan, F., Bertrand, H., & Schaltegger, U. (2020). New high precision U-Pb ages and Hf isotope data from the Karoo large igneous province; implications for pulsed magmatism and early Toarcian environmental perturbations. *Results in Geochemistry*, 1, 100005. <https://doi.org/10.1016/j.ringeo.2020.100005>
- Green, T., Renne, P. R., & Keller, C. B. (2022). Continental flood basalts drive Phanerozoic extinctions. *Proceedings of the National Academy of Sciences of the United States of America*, 119(38), e2120441119. <https://doi.org/10.1073/pnas.2120441119>
- Heimdal, T. H., Goddérís, Y., Jones, M. T., & Svensen, H. H. (2021). Assessing the importance of thermogenic degassing from the Karoo Large Igneous Province (LIP) in driving Toarcian carbon cycle perturbations. *Nature Communications*, 12(1), 6221. <https://doi.org/10.1038/s41467-021-26467-6>
- Hesselbo, S. P., Jenkyns, H. C., Duarte, L. V., & Oliveira, L. C. V. (2007). Carbon-isotope record of the Early Jurassic (Toarcian) Oceanic Anoxic Event from fossil wood and marine carbonate (Lusitanian Basin, Portugal). *Earth and Planetary Science Letters*, 253(3–4), 455–470. <https://doi.org/10.1016/j.epsl.2006.11.009>
- Hetzl, A., Böttcher, M. E., Wortmann, U. G., & Brumsack, H.-J. (2009). Paleo-redox conditions during OAE 2 reflected in Demerara Rise sediment geochemistry (ODP Leg 207). *Palaeogeography, Palaeoclimatology, Palaeoecology*, 273(3–4), 302–328. <https://doi.org/10.1016/j.palaeo.2008.11.005>
- Holland, H. D. (2002). Volcanic gases, black smokers, and the great oxidation event. *Geochimica et Cosmochimica Acta*, 66(21), 3811–3826. [https://doi.org/10.1016/S0016-7037\(02\)00950-X](https://doi.org/10.1016/S0016-7037(02)00950-X)
- Huang, Y., Jin, X., Pancost, R. D., Kemp, D. B., & Naafs, B. D. A. (2024). An intensified lacustrine methane cycle during the Toarcian OAE (Jenkyns Event) in the Ordos Basin, northern China. *Earth and Planetary Science Letters*, 639. <https://doi.org/10.1016/j.epsl.2024.118766>

- Ilyinskaya, E., Mason, E., Wieser, P. E., Holland, L., Liu, E. J., Mather, T. A., Edmonds, M., Whitty, R. C. W., Elias, T., Nadeau, P. A., Schneider, D., McQuaid, J. B., Allen, S. E., Harvey, J., Oppenheimer, C., Kern, C., & Damby, D. (2021). Rapid metal pollutant deposition from the volcanic plume of Kilauea, Hawai'i. *Communications Earth & Environment*, 2(1), 1–16. <https://doi.org/10.1038/s43247-021-00146-2>
- Ishibashi, J. -i., Tsunogai, U., Toki, T., Ebina, N., Gamo, T., Sano, Y., Masuda, H., & Chiba, H. (2015). Chemical composition of hydrothermal fluids in the central and southern Mariana Trough backarc basin. *Deep-Sea Research Part II: Topical Studies in Oceanography*, 121, 126–136. <https://doi.org/10.1016/j.dsr2.2015.06.003>
- James, R. H., Green, D. R. H., Stock, M. J., Alker, B. J., Banerjee, N. R., Cole, C., German, C. R., Huvenne, V. A. I., Powell, A. M., & Connelly, D. P. (2014). Composition of hydrothermal fluids and mineralogy of associated chimney material on the East Scotia Ridge back-arc spreading centre. *Geochimica et Cosmochimica Acta*, 139, 47–71. <https://doi.org/10.1016/j.gca.2014.04.024>
- Jenkyns, H. C. (1988). The early Toarcian (Jurassic) anoxic event; stratigraphic, sedimentary and geochemical evidence. *American Journal of Science*, 288(2), 101–151. <https://doi.org/10.2475/ajs.288.2.101>
- Jenkyns, H. C. (2010). Geochemistry of oceanic anoxic events. *Geochemistry, Geophysics, Geosystems*, 11(3), Q03004. <https://doi.org/10.1029/2009GC002788>
- Ji, F., Zhou, H., Yang, Q., Gao, H., Wang, H., & Lilley, M. D. (2017). Geochemistry of hydrothermal vent fluids and its implications for subsurface processes at the active Longqi hydrothermal field, Southwest Indian Ridge. *Deep Sea Research Part I: Oceanographic Research Papers*, 122, 41–47. <https://doi.org/10.1016/j.dsr.2017.02.001>
- Jiang, Q., Jourdan, F., Olierook, H. K. H., & Merle, R. E. (2023). An appraisal of the ages of Phanerozoic large igneous provinces. *Earth-Science Reviews*, 237, 104314. <https://doi.org/10.1016/j.earscirev.2023.104314>
- Jones, M. T., Jerram, D. A., Svensen, H. H., & Grove, C. (2016). The effects of large igneous provinces on the global carbon and sulphur cycles. *Palaeogeography, Palaeoclimatology, Palaeoecology*, 441, 4–21. <https://doi.org/10.1016/j.palaeo.2015.06.042>
- Kalderon-Asael, B., Katchinoff, J. A. R., Planavsky, N. J., Hood, A. v. S., Dellinger, M., Bellefroid, E. J., Jones, D. S., Hofmann, A., Ossa, F. O., Macdonald, F. A., Wang, C., Isson, T. T., Murphy, J. G., Higgins, J. A., West, A. J., Wallace, M. W., Asael, D., & Pogge von Strandmann, P. A. E. (2021). A lithium-isotope perspective on the evolution of carbon and silicon cycles. *Nature*, 595(7867), 394–398. <https://doi.org/10.1038/s41586-021-03612-1>
- Kasbohm, J., Schoene, B., & Burgess, S. (2021). Radiometric Constraints on the Timing, Tempo, and Effects of Large Igneous Province Emplacement. In *Large Igneous Provinces: A Driver of Global Environmental and Biotic Changes* (pp. 27–82). <https://doi.org/10.1002/9781119507444.ch2>
- Kemp, D. B., Selby, D., & Izumi, K. (2020). Direct coupling between carbon release and weathering during the toarcian oceanic anoxic event. *Geology*, 48(10), 976–980. <https://doi.org/10.1130/G47509.1>
- Kemp, D. B., Suan, G., Fantasia, A., Jin, S., & Chen, W. (2022). Global organic carbon burial during the Toarcian oceanic anoxic event: Patterns and controls. *Earth-Science Reviews*, 231, 104086. <https://doi.org/10.1016/j.earscirev.2022.104086>
- Li, S., Friedrich, O., Nielsen, S. G., Wu, F., & Owens, J. D. (2023). Reconciling biogeochemical redox proxies: Tracking variable bottom water oxygenation during OAE-2 using vanadium isotopes. *Earth and Planetary Science Letters*, 617, 118237. <https://doi.org/10.1016/j.epsl.2023.118237>
- Li, Y.-X., Liu, X., Selby, D., Liu, Z., Montañez, I. P., & Li, X. (2022). Enhanced ocean connectivity and volcanism instigated global onset of Cretaceous Oceanic Anoxic Event 2 (OAE2) ~94.5 million years ago. *Earth and Planetary Science Letters*, 578, 117331. <https://doi.org/10.1016/j.epsl.2021.117331>
- Li, Y.-X., Montañez, I. P., Liu, Z., & Ma, L. (2017). Astronomical constraints on global carbon-cycle perturbation during Oceanic Anoxic Event 2 (OAE2). *Earth and Planetary Science Letters*, 462, 35–46. <https://doi.org/10.1016/j.epsl.2017.01.007>
- Littke, R., Klusmann, U., Krooss, B., & Leythaeuser, D. (1991). Quantification of loss of calcite, pyrite, and organic matter due to weathering of Toarcian black shales and effects on kerogen and bitumen characteristics. *Geochimica et Cosmochimica Acta*, 55(11), 3369–3378. [https://doi.org/10.1016/0016-7037\(91\)90494-P](https://doi.org/10.1016/0016-7037(91)90494-P)
- Lyons, T. W., Reinhard, C. T., & Planavsky, N. J. (2014). The rise of oxygen in Earth's early ocean and atmosphere. *Nature*, 506(7488), 307–315. <https://doi.org/10.1038/nature13068>

- Maher, H. D., Jr. (2001). Manifestations of the Cretaceous High Arctic Large Igneous Province in Svalbard. *The Journal of Geology*, 109(1), 91–104. <https://doi.org/10.1086/317960>
- Mason, E., Wieser, P. E., Liu, E. J., Edmonds, M., Ilyinskaya, E., Whitty, R. C. W., Mather, T. A., Elias, T., Nadeau, P. A., Wilkes, T. C., McGonigle, A. J. S., Perring, T. D., Mims, F. M., Kern, C., Schneider, D. J., & Oppenheimer, C. (2021). Volatile metal emissions from volcanic degassing and lava–seawater interactions at Kilauea Volcano, Hawai'i. *Communications Earth & Environment*, 2(1), 79. <https://doi.org/10.1038/s43247-021-00145-3>
- McArthur, J. M., Donovan, D. T., Thirlwall, M. F., Fouke, B. W., & Matthey, D. (2000). Strontium isotope profile of the early Toarcian (Jurassic) oceanic anoxic event, the duration of ammonite biozones, and belemnite palaeotemperatures. *Earth and Planetary Science Letters*, 179(2), 269–285. [https://doi.org/10.1016/S0012-821X\(00\)00111-4](https://doi.org/10.1016/S0012-821X(00)00111-4)
- McDermott, J. M., Sylva, S. P., Ono, S., German, C. R., & Seewald, J. S. (2018). Geochemistry of fluids from Earth's deepest ridge-crest hot-springs: Piccard hydrothermal field, Mid-Cayman Rise. *Geochimica et Cosmochimica Acta*, 228, 95–118. <https://doi.org/10.1016/j.gca.2018.01.021>
- Meyer, K. M., & Kump, L. R. (2008). Oceanic euxinia in Earth history: Causes and consequences. *Annual Review of Earth and Planetary Sciences*, 36(1), 251–288. <https://doi.org/10.1146/annurev.earth.36.031207.124256>
- Meyers, S. R., Siewert, S. E., Singer, B. S., Sageman, B. B., Condon, D. J., Obradovich, J. D., Jicha, B. R., & Sawyer, D. A. (2012). Intercalibration of radioisotopic and astrochronologic time scales for the Cenomanian-Turonian boundary interval, western interior Basin, USA. *Geology*, 40(1), 7–10. <https://doi.org/10.1130/G32261.1>
- Misra, S., & Froelich, P. N. (2012). Lithium isotope history of cenozoic seawater: Changes in silicate weathering and reverse weathering. *Science*, 335(6070), 818–823. <https://doi.org/10.1126/science.1214697>
- Miyazaki, Y., Planavsky, N. J., Bolton, E. W., & Reinhard, C. T. (2018). Making sense of massive carbon isotope excursions with an inverse carbon cycle model. *Journal of Geophysical Research: Biogeosciences*, 123(8), 2485–2496. <https://doi.org/10.1029/2018JG004416>
- Montoya-Pino, C., Weyer, S., Anbar, A. D., Pross, J., Oschmann, W., van de Schootbrugge, B., & Arz, H. W. (2010). Global enhancement of ocean anoxia during Oceanic Anoxic Event 2: A quantitative approach using U isotopes. *Geology*, 38(4), 315–318. <https://doi.org/10.1130/G30652.1>
- Morten, S. D., & Twitchett, R. J. (2009). Fluctuations in the body size of marine invertebrates through the Pliensbachian-Toarcian extinction event. *Palaeogeography, Palaeoclimatology, Palaeoecology*, 284(1–2), 29–38. <https://doi.org/10.1016/j.palaeo.2009.08.023>
- Nielsen, S. G., Rehkämper, M., Teagle, D. A. H., Butterfield, D. A., Alt, J. C., & Halliday, A. N. (2006). Hydrothermal fluid fluxes calculated from the isotopic mass balance of thallium in the ocean crust. *Earth and Planetary Science Letters*, 251(1–2), 120–133. <https://doi.org/10.1016/j.epsl.2006.09.002>
- Nordt, L., Breecker, D., & White, J. (2022). Jurassic greenhouse ice-sheet fluctuations sensitive to atmospheric CO₂ dynamics. *Nature Geoscience*, 15(1), 54–59. <https://doi.org/10.1038/s41561-021-00858-2>
- Ostrander, C. M., Owens, J. D., & Nielsen, S. G. (2017). Constraining the rate of oceanic deoxygenation leading up to a Cretaceous Oceanic Anoxic Event (OAE-2: ~94 Ma). *Science Advances*, 3(8), e1701020. <https://doi.org/10.1126/sciadv.1701020>
- Owens, J. D., Gill, B. C., Jenkyns, H. C., Bates, S. M., Severmann, S., Kuypers, M. M. M., Woodfine, R. G., & Lyons, T. W. (2013). Sulfur isotopes track the global extent and dynamics of euxinia during Cretaceous Oceanic Anoxic Event 2. *Proceedings of the National Academy of Sciences*, 110(46), 18407–18412. <https://doi.org/10.1073/pnas.1305304110>
- Owens, J. D., Lyons, T. W., & Lowery, C. M. (2018). Quantifying the missing sink for global organic carbon burial during a Cretaceous oceanic anoxic event. *Earth and Planetary Science Letters*, 499, 83–94. <https://doi.org/10.1016/j.epsl.2018.07.021>
- Owens, J. D., Reinhard, C. T., Rohrssen, M., Love, G. D., & Lyons, T. W. (2016). Empirical links between trace metal cycling and marine microbial ecology during a large perturbation to Earth's carbon cycle. *Earth and Planetary Science Letters*, 449, 407–417. <https://doi.org/10.1016/j.epsl.2016.05.046>
- Pálffy, J., & Smith, P. L. (2000). Synchrony between Early Jurassic extinction, oceanic anoxic event, and the Karoo-Ferrar flood basalt volcanism. *Geology*, 28(8), 747–750. [https://doi.org/10.1130/0091-7613\(2000\)28](https://doi.org/10.1130/0091-7613(2000)28)

- Percival, L. M. E., Cohen, A. S., Davies, M. K., Dickson, A. J., Hesselbo, S. P., Jenkyns, H. C., Leng, M. J., Mather, T. A., Storm, M. S., & Xu, W. (2016). Osmium isotope evidence for two pulses of increased continental weathering linked to Early Jurassic volcanism and climate change. *Geology*, 44(9), 759–762. <https://doi.org/10.1130/G37997.1>
- Percival, L. M. E., Witt, M. L. I., Mather, T. A., Hermoso, M., Jenkyns, H. C., Hesselbo, S. P., Al-Suwaidi, A. H., Storm, M. S., Xu, W., & Ruhl, M. (2015). Globally enhanced mercury deposition during the end-Pliensbachian extinction and Toarcian OAE: A link to the Karoo-Ferrar Large Igneous Province. *Earth and Planetary Science Letters*, 428, 267–280. <https://doi.org/10.1016/j.epsl.2015.06.064>
- Petsch, S. T., Berner, R. A., & Eglinton, T. I. (2000). A field study of the chemical weathering of ancient sedimentary organic matter. *Organic Geochemistry*, 31(5), 475–487. [https://doi.org/10.1016/S0146-6380\(00\)00014-0](https://doi.org/10.1016/S0146-6380(00)00014-0)
- Pogge von Strandmann, P. A. E., Cosford, L. R., Liu, C.-Y., Liu, X., Krause, A. J., Wilson, D. J., He, X., McCoy-West, A. J., Gislason, S. R., & Burton, K. W. (2023). Assessing hydrological controls on the lithium isotope weathering tracer. *Chemical Geology*, 642, 121801. <https://doi.org/10.1016/j.chemgeo.2023.121801>
- Pogge von Strandmann, P. A. E., Jenkyns, H. C., & Woodfine, R. G. (2013). Lithium isotope evidence for enhanced weathering during Oceanic Anoxic Event 2. *Nature Geoscience*, 6(8), 668–672. <https://doi.org/10.1038/ngeo1875>
- Poulton, S. W., Henkel, S., März, C., Urquhart, H., Flögel, S., Kasten, S., Sinninghe Damsté, J. S., & Wagner, T. (2015). A continental-weathering control on orbitally driven redox-nutrient cycling during Cretaceous oceanic anoxic event 2. *Geology*, 43(11), 963–966. <https://doi.org/10.1130/G36837.1>
- Raven, M. R., Fike, D. A., Bradley, A. S., Gomes, M. L., Owens, J. D., & Webb, S. A. (2019). Paired organic matter and pyrite $\delta^{34}\text{S}$ records reveal mechanisms of carbon, sulfur, and iron cycle disruption during Ocean Anoxic Event 2. *Earth and Planetary Science Letters*, 512, 27–38. <https://doi.org/10.1016/j.epsl.2019.01.048>
- Reershemius, T., & Planavsky, N. J. (2021). What controls the duration and intensity of ocean anoxic events in the Paleozoic and the Mesozoic? *Earth-Science Reviews*, 221, 103787. <https://doi.org/10.1016/j.earscirev.2021.103787>
- Reeves, E. P., Seewald, J. S., Saccocia, P., Bach, W., Craddock, P. R., Shanks, W. C., Sylva, S. P., Walsh, E., Pichler, T., & Rosner, M. (2011). Geochemistry of hydrothermal fluids from the PACMANUS, Northeast Pual and Vienna Woods hydrothermal fields, Manus Basin, Papua New Guinea. *Geochimica et Cosmochimica Acta*, 75(4), 1088–1123. <https://doi.org/10.1016/j.gca.2010.11.008>
- Reinhard, C. T., & Planavsky, N. J. (2022). The History of Ocean Oxygenation. *Annual Review of Marine Science*, 14(1), 331–353. <https://doi.org/10.1146/annurev-marine-031721-104005>
- Reinhard, C. T., Planavsky, N. J., Robbins, L. J., Partin, C. A., Gill, B. C., Lalonde, S. V., Bekker, A., Konhauser, K. O., & Lyons, T. W. (2013). Proterozoic ocean redox and biogeochemical stasis. *Proceedings of the National Academy of Sciences of the United States of America*, 110(14), 5357–5362. <https://doi.org/10.1073/pnas.1208622110>
- Riebe, C. S., Kirchner, J. W., & Finkel, R. C. (2003). Long-term rates of chemical weathering and physical erosion from cosmogenic nuclides and geochemical mass balance. *Geochimica et Cosmochimica Acta*, 67(22), 4411–4427. [https://doi.org/10.1016/S0016-7037\(03\)00382-X](https://doi.org/10.1016/S0016-7037(03)00382-X)
- Riebe, C. S., Kirchner, J. W., & Finkel, R. C. (2004). Erosional and climatic effects on long-term chemical weathering rates in granitic landscapes spanning diverse climate regimes. *Earth and Planetary Science Letters*, 224(3–4), 547–562. <https://doi.org/10.1016/j.epsl.2004.05.019>
- Ruebsam, W., Reolid, M., Mattioli, E., & Schwark, L. (2022). Organic carbon accumulation at the northern Gondwana paleomargin (Tunisia) during the Toarcian Oceanic Anoxic Event: Sedimentological and geochemical evidence. *Palaeogeography, Palaeoclimatology, Palaeoecology*, 586, 110781. <https://doi.org/10.1016/j.palaeo.2021.110781>
- Ruebsam, W., & Schwark, L. (2024). Disparity between Toarcian Oceanic Anoxic Event and Toarcian carbon isotope excursion. *International Journal of Earth Sciences*, 113(8), 2065–2076. <https://doi.org/10.1007/s00531-024-02408-8>
- Saltzman, M. R., Young, S. A., Kump, L. R., Gill, B. C., Lyons, T. W., & Runnegar, B. (2011). Pulse of atmospheric oxygen during the late Cambrian. *Proceedings of the National Academy of Sciences of the United States of America*, 108(10), 3876–3881. <https://doi.org/10.1073/pnas.1011836108>
- Schlanger, S., & Jenkyns, H. (1976). Cretaceous oceanic anoxic event cause an consequences. *Geologie En Mijnbouw*, 55(3–4), 179–184. <https://ora.ox.ac.uk/objects/uuid:0921605b-4793-43df-889d-7b896790de62>

- Self, S., Blake, S., Sharma, K., Widdowson, M., & Sephton, S. (2008). Sulfur and Chlorine in Late Cretaceous. *Science*, 319(5870), 1654–1657. <https://doi.org/10.1126/science.11528>
- Seyfried, W. E., Jr., Pester, N. J., Tutolo, B. M., & Ding, K. (2015). The Lost City hydrothermal system: Constraints imposed by vent fluid chemistry and reaction path models on seafloor heat and mass transfer processes. *Geochimica et Cosmochimica Acta*, 163, 59–79. <https://doi.org/10.1016/j.gca.2015.04.040>
- Sinton, C. W., & Duncan, R. A. (1997). Potential links between ocean plateau volcanism and global ocean anoxia at the Cenomanian-Turonian Boundary. *Economic Geology*, 92, 836–842. <https://doi.org/10.2113/gsecongeo.92.7-8.836>
- Sullivan, D. L., Brandon, A. D., Eldrett, J., Bergman, S. C., Wright, S., & Minisini, D. (2020). High resolution osmium data record three distinct pulses of magmatic activity during cretaceous Oceanic Anoxic Event 2 (OAE-2). *Geochimica et Cosmochimica Acta*, 285, 257–273. <https://doi.org/10.1016/j.gca.2020.04.002>
- Them, T. R., Gill, B. C., Selby, D., Gröcke, D. R., Friedman, R. M., & Owens, J. D. (2017). Evidence for rapid weathering response to climatic warming during the Toarcian Oceanic Anoxic Event. *Scientific Reports*, 7(1), 5003. <https://doi.org/10.1038/s41598-017-05307-y>
- Them, T. R., II, Gill, B. C., Caruthers, A. H., Gerhardt, A. M., Gröcke, D. R., Lyons, T. W., Marroquín, S. M., Nielsen, S. G., João, P. T. A., & Owens, J. D. (2018). Thallium isotopes reveal protracted anoxia during the Toarcian (Early Jurassic) associated with volcanism, carbon burial, and mass extinction. *Proceedings of the National Academy of Sciences of the United States of America*, 115(26), 6596–6601. <https://doi.org/10.1073/pnas.1803478115>
- Them, T. R., II, Gill, B. C., Caruthers, A. H., Gröcke, D. R., Tulskey, E. T., Martindale, R. C., Poulton, T. P., & Smith, P. L. (2017). High-resolution carbon isotope records of the Toarcian Oceanic Anoxic Event (Early Jurassic) from North America and implications for the global drivers of the Toarcian carbon cycle. *Earth and Planetary Science Letters*, 459, 118–126. <https://doi.org/10.1016/j.epsl.2016.11.021>
- Them, T. R., II, Owens, J. D., Marroquín, S. M., Caruthers, A. H., Alexandre, J. P. T., & Gill, B. C. (2022). Reduced Marine Molybdenum Inventory Related to Enhanced Organic Carbon Burial and an Expansion of Reducing Environments in the Toarcian (Early Jurassic) Oceans. *AGU Advances*, 3(6), e2022AV000671. <https://doi.org/10.1029/2022AV000671>
- Van Cappellen, P., & Ingall, E. D. (1994). Benthic phosphorus regeneration, net primary production, and ocean anoxia: A model of the coupled marine biogeochemical cycles of carbon and phosphorus. *Paleoceanography*, 9(5), 677–692. <https://doi.org/10.1029/94PA01455>
- Von Damm, K. L. (1990). Seafloor hydrothermal activity: black smoker chemistry and chimneys. *Annual Review of Earth and Planetary Sciences*, 18(1), 173–204. <https://doi.org/10.1146/annurev.ea.18.050190.001133>
- Wignall, P. B., Bond, D. P. G., Kuwahara, K., Kakuwa, Y., Newton, R. J., & Poulton, S. W. (2010). An 80 million year oceanic redox history from Permian to Jurassic pelagic sediments of the Mino-Tamba terrane, SW Japan, and the origin of four mass extinctions. *Global and Planetary Change*, 71(1–2), 109–123. <https://doi.org/10.1016/j.gloplacha.2010.01.022>
- Wignall, P. B., Hallam, A., Newton, R. J., Sha, J. G., Reeves, E., Mattioli, E., & Crowley, S. (2006). An eastern Tethyan (Tibetan) record of the Early Jurassic (Toarcian) mass extinction event. *Geobiology*, 4(3), 179–190. <https://doi.org/10.1111/j.1472-4669.2006.00081.x>
- Xu, W., Ruhl, M., Jenkyns, H. C., Hesselbo, S. P., Riding, J. B., Selby, D., Naafs, B. D. A., Weijers, J. W. H., Pancost, R. D., Tegelaar, E. W., & Idiz, E. F. (2017). Carbon sequestration in an expanded lake system during the Toarcian oceanic anoxic event. *Nature Geoscience*, 10(2), 129–134. <https://doi.org/10.1038/ngeo2871>

SUPPLEMENTARY MATERIALS

Balancing redox budgets: Mechanisms for prolonging anoxia during major carbon burial events (supplemental)

Download: <https://ajsonline.org/article/143665-balancing-redox-budgets-mechanisms-for-prolonging-anoxia-during-major-carbon-burial-events/attachment/299667.docx>
